Abstract

CLARK, BRANDON RICHARD. Real-time Fusion Power Monitor via Neutron Activation of Circulating Fluid. (Under the direction of Mohammed A. Bourham.)

Much effort has been devoted to the concept of fusion reactors, both magnetic and inertial confinement, to pursue an alternative source of energy. The concept of tokamaks have shown the most promising in magnetic confinement fusion, and thus an international effort has combined the expertise of the scientific community to build the first test reactor in southern France. The International Thermonuclear Experimental Reactor (ITER) will employ a diagnostic tool which circulates a fluid that is activated by the fusion neutrons. The activated fluid is then monitored by a detector, whose resulting data is used to infer the fusion power.

This work set out to computationally apply the same design theory to the General Atomics DIII-D toroidal fusion reactor, located in La Jolla, California. With a careful choice for the irradiation site, the device should be able to both accurately infer fusion power and the neutron flux incident upon material samples. Monte Carlo simulations were employed to determine the activation yield, as well as the best detector geometry and resulting detection yield. Other components such as delay tank, heater, and pump are either discussed or investigated. A FORTRAN program was created to compute fusion power from detector output in such a way that the device can be operated in 'near' real-time with minimal delays resulting from fluid circulation and numerical techniques. Computational analysis has shown that such a device is feasible, and thus has also laid a solid foundation for experimental application.

Real-time Fusion Power Monitor via Neutron Activation of Circulating Fluid

by

Brandon Richard Clark

A thesis submitted to the Graduate Faculty of
North Carolina State University
in partial fulfillment of the
requirements for the Degree of
Master of Science

Nuclear Engineering

Raleigh, North Carolina
2007

Approved By:

Dr. Mohamed A. Bourham (Chair of Advisory Committee)	Dr. Robin P. Gardner
Dr. Dmitriy Y. Anistratov	Dr. Gary E. Mitchell (Minor Representative)

Biography

Brandon Richard Clark was born on February 12, 1984, to Richard and Diane Clark; born and raised in Concord, North Carolina, with his brother, Justin. Education and learning were never interests during his younger years. Instead, the days were spent playing sports with the neighborhood friends, playing video games with Justin, or building some fort of some kind. His earliest career plan was to become a professional basketball player, but fate was not kind enough to such a dream, and soon his career interests focused on his other passion, helping animals and nature. The idea of spending his future as a veterinarian entertained him until his freshman year of high school.

In December of his freshman year of high school, Brandon read *Journey Across the Subatomic Cosmos*, by Isaac Asimov, simply out of curiosity. That book opened his mind to concepts and ideas that would drive his imagination for years to come. Over the following few years, his subatomic interests focused closer on the nucleus and nuclear reactions. After a three week nuclear engineering summer camp at NC State University he was completely sold on the idea of becoming a nuclear engineer; thus, he enrolled in the nuclear engineering program at NC State following graduation from high school. After earning his BS in nuclear engineering he continued his education through the accelerated MS program. Brandon is currently employed with Duke Energy at their Catawba nuclear plant, with their Reactor Engineering group.

Acknowledgments

First, I would like to thank Dr. M. A. Bourham for accepting my offer to advise me through my Masters work. His guidance and encouragement have kept me motivated throughout the process. As well, his efforts to mentor me as both an undergraduate, and as a high school student, have helped to make my academic career both enjoyable and successful.

I would like to also acknowledge the time and effort of Dr. R. P. Gardner. His expertise in nuclear instruments and circulating fluid diagnostics has been very indispensable. And it can not be left out that his assistance was notably prompt, in-depth, and inspiring.

The exhaustive effort of Dr. D. Y. Anistratov in helping me determine my thesis topic is well appreciated. I would also like to thank Dr. G. E. Mitchell for accepting my offer to represent my physics minor.

I was fortunate to have the help of many experts along the way. Notably: Dr. Clement Wong and Peter Taylor of the DIII-D group, Dr. Libai Xu for MCNP help, the active members of the MCNP Forum, and Saint-Gobain for detector specifications. And last, but not least, my friend Paul Swaney for entertaining and motivating me throughout.

Table of Contents

List of Tables

List of Figures

1 Introduction

1.1 Radiation and Interaction with Matter

The nucleus of an atom can become unstable by the capture of a neutron, or another subatomic particle. In fact, scientists and engineers have successfully spent the last century finding new ways to exploit this fact for the betterment of mankind. Although this research does not setout to save lives, radiation and nuclear instability are once again the primary participants. To understand the concept of an activation based power monitoring device, one must first understand radiation and nuclear instability. For reasons that will be revealed later, it is relevant to limit the discussion to neutron capture and beta/gamma emission.

For a nucleus to capture a neutron, it must directly interact with it, seeing as Coulomb forces are not an option. The probability of interaction scales proportionally with the cross-section. Denoted by σ, and carrying units of area, it is not difficult to see that σ is nothing more than the effective cross-sectional area of the nucleus, hence the term cross-section [1]. When a nucleus absorbs a neutron it may become a whole new atom (i.e. different atomic number) or it may remain the same atom, either way the nucleus is very well likely to become unstable.

Once unstable, a nucleus will undergo a nuclear reaction, or a series of nuclear reactions, in an effort to stabilize itself. Two common forms of nuclear reactions are beta emission and gamma emission. Beta particles are essentially electrons ejected from the nucleus, and gamma rays are photons (energy packets) also ejected from the nucleus. By releasing energy in the form of beta or gamma emission, the nucleus attempts to return to a stable state. However, the ejection is rarely monoenergetic, which consequently leads to a decay spectrum where some energy is released via beta emission and some by gamma. Thankfully, these spectrums are quite

unique for each isotope and well tabulated, thus allowing for the development of devices and techniques based on these tabulated properties.

The probability of emission can be quantized by the half-life, $t_{1/2}$, which is the time required for half of an arbitrary amount of a radioactive isotope to decay away (i.e. undergo nuclear reactions). When the nucleus decays it either retains its atomic number, and thus chemical identity, or it becomes a new atom. No matter how much time this process takes, or how much radiation is emitted, the end result is a stable isotope.

1.2 Fusion, DIII-D, and DiMES

Fusion occurs when two nuclei are brought close enough together that the weak nuclear force begins to dominate, uniting the two nuclei, forming a new nucleus and new atom and releases energy. The difficulty in fusion is creating a device that can control the fusion, while also transferring enough energy to the nuclei to overcome the Columbic force of repulsion between the two interacting positively charged nuclei. As mentioned above, during the fusion process energy is released and thus decreasing, and possibly eliminating, the supplemental amount needed to sustain the fusion process [2].

One way to contain the fusion process, in which the plasma core is very hot (several keV), is by the use of a magnetic confinement device, employing what is known as magnetic confinement fusion (MCF). For such a device, the formation of hot plasma (essentially a collection of ionized gas molecules) is crucial to induce fusion in which the ions of light nuclei (hydrogen isotopes) fuse together. Since the fuel species (deuterium and tritium) are ionized, it is then possible to confine the ionic species by electromagnetic means. An MCF device, such as a tokamak, employs magnetic fields to confine the charged particles and imposes magnetic

pressure to pinch the plasma towards the center, thus fusing the ions. The main reason for the MCF devices taking the toroidal shape is to confine the charged particles between each of the two coil systems, known as magnetic mirror, and thus prevent plasma from escaping as the end effects would be eliminated. It is also important to mention that toroidal plasma has a stability index with respect to the balance between magnetic field pressure and plasma kinetic pressure, and the plasma is more stable in a toroidally-shaped configuration. In a linear plasma system, plasma will escape from the ends of the confining magnetic fields due to the end effects [2].

The ultimate goal of MCF is an efficient, aneutronic, fusion reactor that safely produces electricity, and there is much research to be performed before this goal can be realized. Fusion power efficiency has made amazing progress since the 1970s, when toroidal MCF devices were first realized. A fact shown clearly in Figure 1.2.1, in which several fusion experimental devices advanced towards ignition criteria. It is clearly visible from Figure 1.2.1 that MCF advancements are well comparable to the progress shown by computer chip memory technological advancement. This is due largely to the better understanding of magnetically confined plasma, as well as the large progress made in material development [2].

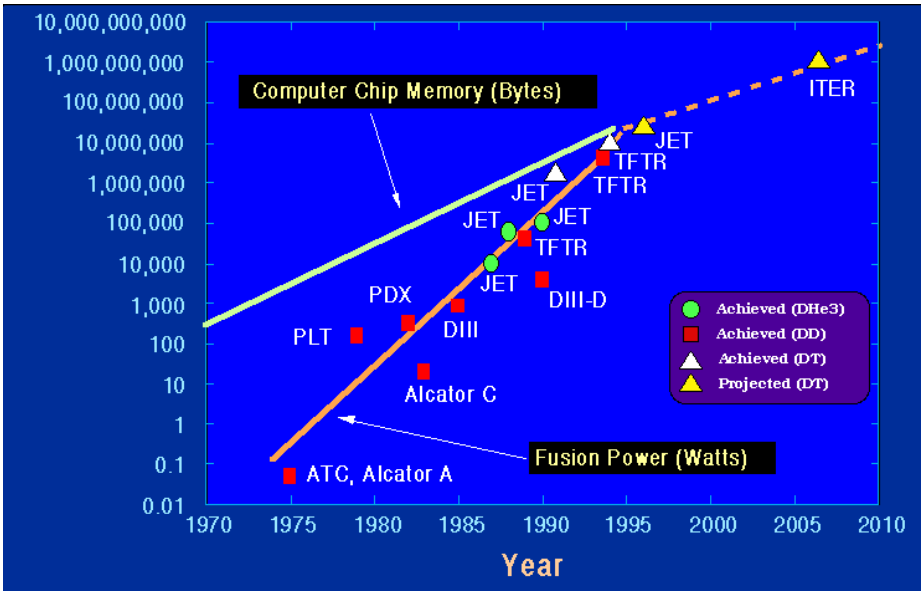

Figure 1.2.1: Fusion power increase
Taken from Ref. [3] - Fusion Technology Institute. 15 Mar 2007. <http://fti.neep.wisc.edu/neep602/LEC24/IMAGES/Fusion.GIF>

Aneutronic fusion posses the advantage over neutronic fusion in that material irradiation and personnel radiation exposure are minimized or completely overcome. However, MCF will need to increase much more in power before such higher atomic number nuclei can be fused. This fact is evident by observing a binding energy per nucleon graph, such as shown in Figure 1.2.2.

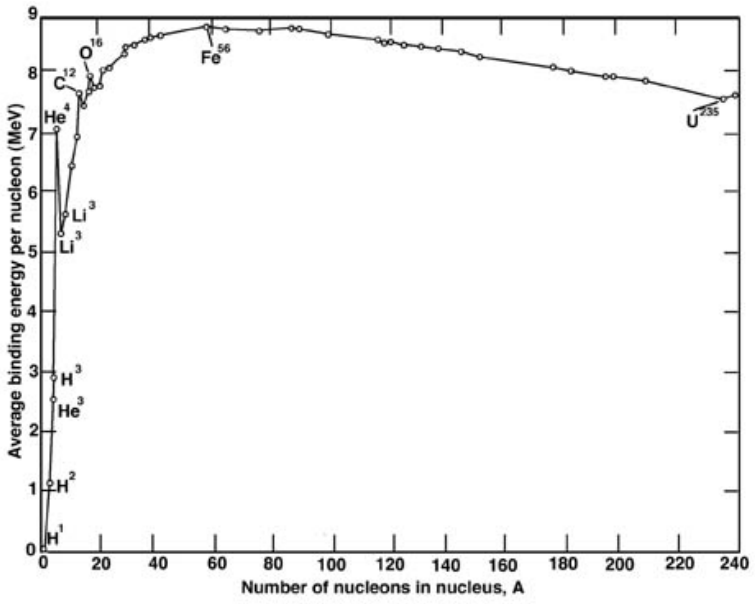

Figure 1.2.2: Average binding energy per nucleon
Taken from Ref. [4] - NASA. 15 Mar 2007.
<http://imagine.gsfc.nasa.gov/Images/teachers/posters/elements/booklet/energy.jpg>

For now the nucleons with lower average binding energies can only be considered for fusion, and thus the hydrogen isotopes and ^{3}He are the possible fusion fuel species. There are currently two fusion schemes that are of interest for the first generation fusion reactors. The first is the fusion reaction between two heavy hydrogen isotopes, referred to as "deuterium" (^{2}H or D), and the second is between deuterium and tritium (^{3}H or T).

$$\begin{aligned} D + D &\rightarrow T \quad + p \\ &\rightarrow {}^3He + n \\ D + T &\rightarrow {}^4He + n \end{aligned}$$

Where the D-D neutron in the second possible branch of reaction ($D + D \rightarrow {}^3He + n$) carries 2.45MeV, and the D-T neutron in the reaction ($D + T \rightarrow {}^4He + n$) carries 14.1MeV.

The latest activity in magnetic fusion test reactors is the design of the International Thermonuclear Experimental Reactor (ITER). As Figure 1.2.1 shows, ITER is expected to serve as the first experimental fusion test reactor that directly leads towards commercial reactors later

on. Currently, the parties supporting ITER are the European Union, Japan, the Peoples' Republic of China, India, the Republic of Korea, the Russian Federation, and the United States of America [5]. ITER will function as the main research vessel before an actual DEMO is constructed.

An MCF reactor that has contributed significantly to the scientific community, and to ITER's research development and design activities, is the DIII-D; developed and operated by General Atomics and located in Sorrento Valley, California [6]. A cartoon of the DIII-D is below:

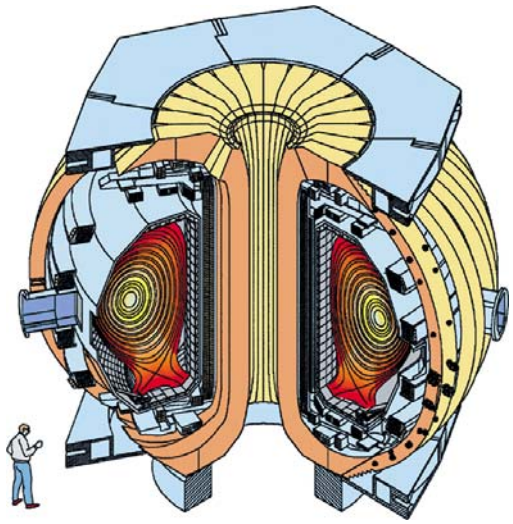

Figure 1.2.3: DIII-D Fusion Reactor
Taken from Ref. [7] - SolidWorks Express. 5 Mar 2007.
<http://www.solidworks.com/swexpress/pages/mar05/PU_GeneralAtomics.html>

As seen from the concentric circles in Figure 1.2.3; plasma temperature is highest at the center of these circles, which represent the core of the fusion reactor. The DIII-D currently employs the D-D scheme, although the D-T scheme is likely to be integrated in the near future [8]. Once the change is made to D-T, some design features will also change; notable the activation substance. The fuel for the DIII-D takes the form of a small pellet. These pellets are injected from the top of the device at very high speeds [9]. The high injection speeds are necessary because the

plasma erodes the fuel at a high rate, thus for the fuel pellet to reach the center of the plasma, where it must reach for the fusion occur, high speeds are needed before it falls apart or is consumed and ablated during its travel to the core. The portion of the pellet that reaches the center is burned via the fusion process, specifically the D-D scheme. There is enough fuel for the DIII-D to burn for approximately five seconds; referred to as a "shot." Typical DIII-D shot characteristics are summarized in Table 1.2.1. The neutrons produced during the shot radiate symmetrically in all direction from their origin.

Table 1.2.1: DIII-D shot properties [10]

Maximum Neutron Emission Rate	1×10^{16} n/s
Maximum Neutron Emission	2×10^{16} n/shot
Shot Length	5 second
Time Between Consecutive Shots	10-15 minutes

The DIII-D is a research device and thus it has integrated a lot of diagnostic and experimental hardware. One important piece of hardware is the Divertor Material Evaluation System (DiMES) [11]. The main purpose of DiMES is to test various materials on how well they hold up to the challenging conditions found within the DIII-D vessel, specifically the performance with respect to high heat flux deposition, erosion and surface ablation, degradation, nucleation and survivability under abnormal conditions such as hard disruptions and accident scenarios. This will help future MCF reactors integrate the optimum material for their inner vessel wall. Setup includes placing a prefabricated sample into the DiMES and then bringing to its testing position, which is where the sample forms part of the reactor vessel wall. The DiMES sample has a partial "bubble" on it that protrudes into the vessel, increasing the interaction between the sample and the flowing ash layer plasma. After exposed to a set number of shots, the sample is then analyzed to determine the effect of plasma-material interaction and to evaluate

different materials for possible integration into the device. This research will utilize the DiMES by setting a fluid irradiation volume within the DiMES sample for use in the neutron activation analysis as means by which the fusion power can be monitored in real-time.

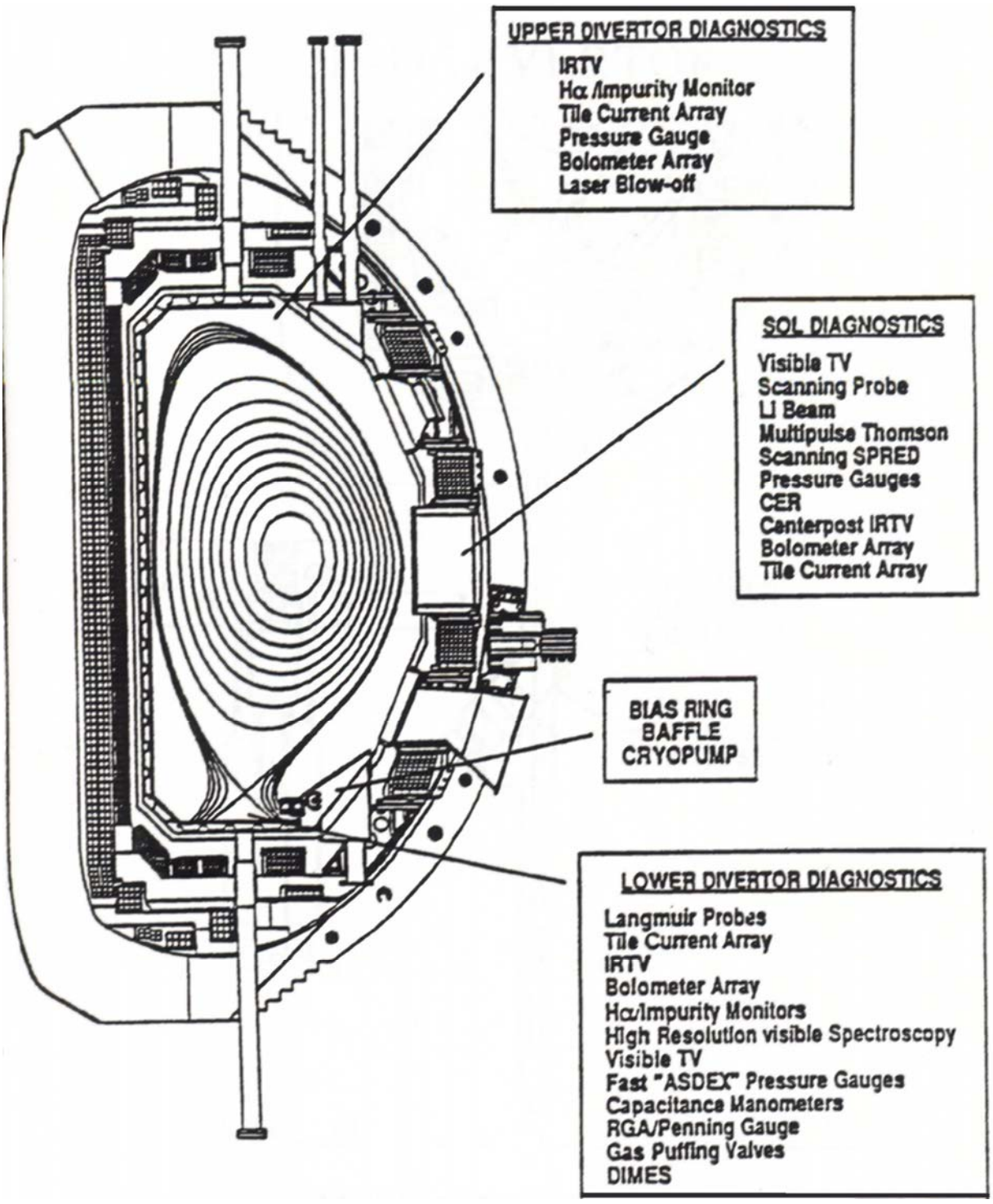

Figure 1.2.4: DIII-D cross-section with diagnostic instrument listing
Taken from Ref. [12] - Nahm, Meredith and Crystal Buchanan. "Design of Multi-Diagnostic Dimes." Senior design. Spring 1993.

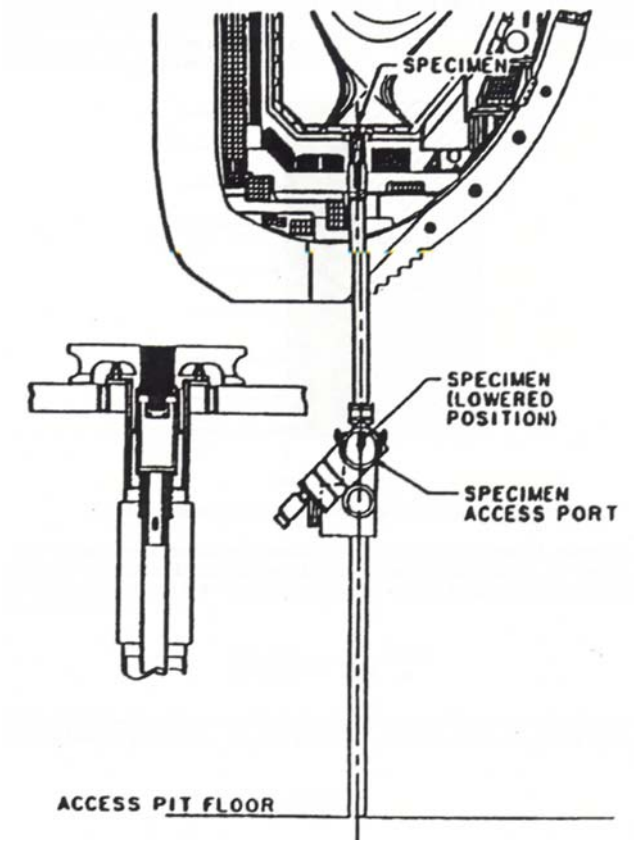

Figure 1.2.5: DiMES device
Taken from Ref. [12] - Nahm, Meredith and Crystal Buchanan. "Design of Multi-Diagnostic Dimes." Senior design. Spring 1993.

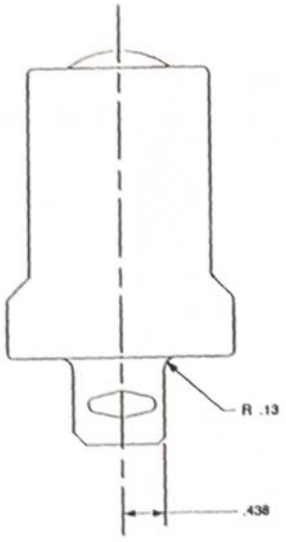

Figure 1.2.6: DiMES sample cross-section
Taken from Ref. [12] - Nahm, Meredith and Crystal Buchanan. "Design of Multi-Diagnostic Dimes." Senior design. Spring 1993.

1.3 Scope and Purpose of the Work

The purpose of this research is to design a device that will measure the fusion power of the DIII-D in real-time by measuring the level of activation of a circulating fluid. The fluid is to be circulated through the DiMES sample, thus modification is necessary to the sample and the DiMES housing to integrate the circulating fluid system into the existing DiMES. Since the irradiation site is within the DiMES sample, it is also possible to measure the neutron flux incident upon the sample, providing an extra degree of study. The scope is limited to a computational/analytical viewpoint with comments provided on actual application. Radiation yields are determined by use of the MCNP5 computer code. A computer code is developed to "backtrack" detector counts to fusion power in real-time. This research is intended to provide a solid foundation for applying such a device to the DIII-D and scaling to other fusion devices. Also this research is possibly applicable to any neutron emitting source.

1.4 Literature Survey

ITER will employ a power monitoring device based on neutron activation of a flowing fluid [13]. Some preliminary research has been performed to determine the technical feasibility of such a device. A team at the Japan Atomic Energy Research Institute (JAERI) performed a particularly interesting experiment. ITER will burn D-T fuel pellets, thus for reasons shown later, the JAERI team used H_2O as their circulating fluid. A schematic of their experimental setup is shown in Figure 1.4.1. As is shown, water begins in the reservoir and is then pumped through plastic tubing to the irradiation site, where plastic tubing is replaced by steel tubing. The water is then circulated back through the shielding wall, where it is analyzed by the isolated

BGO Scintillation detector. Finally, the water returns to the reservoir after passing through the flow meter.

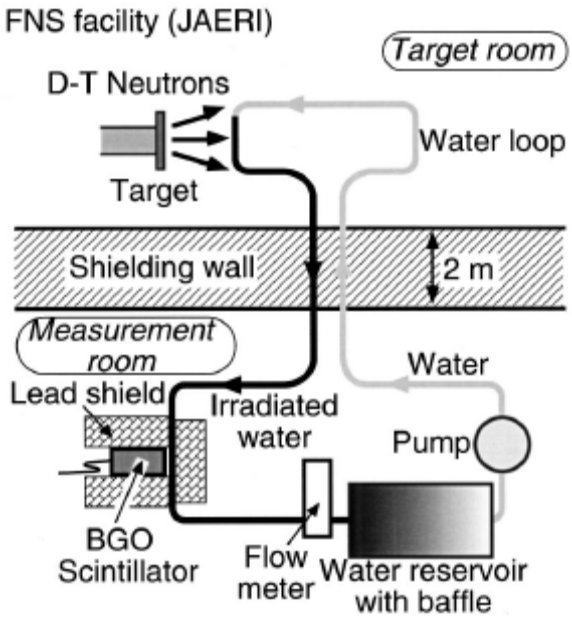

Figure 1.4.1: JAERI experimental setup
Taken from Ref [13] - Kaneko, Junichi, Yoshitomo Uno, Takeo Nishitani, Fujio Maekawa, Teruya Tanaka, Yoshinari Shibata, Yujiro Ikeda, and Hiroshi Takeuchi. "Technical feasibility study on a fusion power monitor based on activation of water flow." Review of Scientific Instruments. 72.1 (January 2001).

The research performed by the JAERI team looked mainly at whether such a device could meet the ITER time resolution requirement of 100ms. They also investigated the ^{16}N gamma yield on the velocity of the flowing water. They concluded that the time response was modeled best by turbulent flow and that a time resolution of 100ms could easily be met.

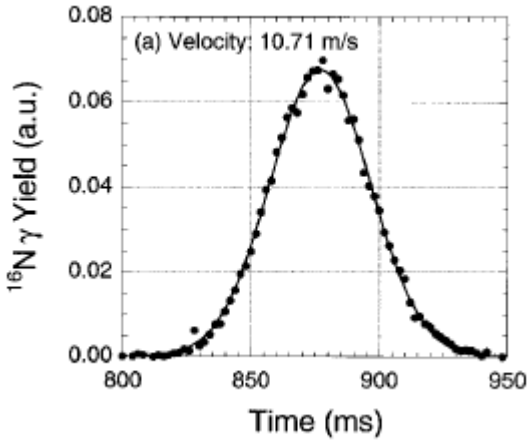

Figure 1.4.2: JAERI ^{16}N gamma yield dependence on time for turbulent flow
Taken from Ref [13] - Kaneko, Junichi, Yoshitomo Uno, Takeo Nishitani, Fujio Maekawa, Teruya Tanaka, Yoshinari Shibata, Yujiro Ikeda, and Hiroshi Takeuchi. "Technical feasibility study on a fusion power monitor based on activation of water flow." Review of Scientific Instruments. 72.1 (January 2001).

The accurate fitting of experimental data to the model shown in Figure 1.4.2 indicates turbulent flow is optimal; which also carries over into this research's design. Another fact that will carry over from the work performed by JAERI is that time resolution is minimized when the traveling time of the fluid between irradiation and the detector is minimized. This can be expected since turbulent flow is optimal (i.e. high flow velocity).

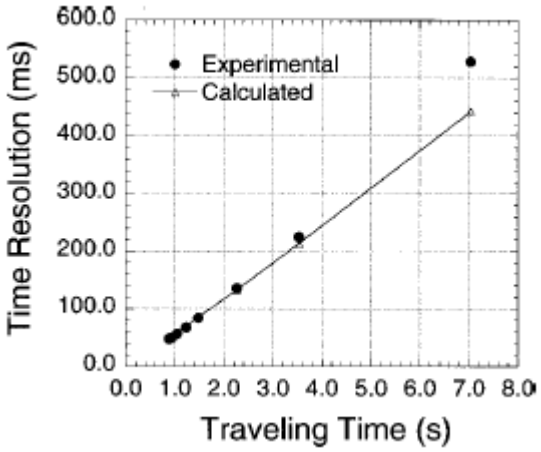

Figure 1.4.3: JAERI time resolution dependence on traveling time
Taken from Ref [13] - Kaneko, Junichi, Yoshitomo Uno, Takeo Nishitani, Fujio Maekawa, Teruya Tanaka, Yoshinari Shibata, Yujiro Ikeda, and Hiroshi Takeuchi. "Technical feasibility study on a fusion power monitor based on activation of water flow." Review of Scientific Instruments. 72.1 (January 2001).

In private communication with ITER's research personal, it was found that the actual device for ITER has not yet been designed [14].

There has also been research performed at NC State University on a general model for continuous on-stream neutron activation analysis [15]. Although distinctly different than this research, the work helps to provide some mathematical insight as well as an assumption known as "perfect mixing," which improves the design. Their research had the unpleasantry of dealing with radionuclide recirculation, and thus buildup. This difficulty does not transfer since the design here implements a delay tank, which rids the recirculated fluid of most all radionuclides.

2 Preliminary View of Design, Components, Constraints, and Analysis

2.1 Design Overview

The design is simple and consists of a small number of components, all of which are easily available for a relatively cheap price.

Beginning at the delay tank, the non-radioactive fluid will travel to the modified DiMES sample to allow for fluid circulation into and out from the DiMES. Once the fluid is out of the DiMES sample, the irradiated fluid will then travel to the detector, where count-rate will be recorded at constant intervals of time. After leaving the detector, the fluid will travel back to the delay tank, where enough time will elapse such that the fluid can be considered non-radioactive when it leaves the delay tank to repeat its journey.

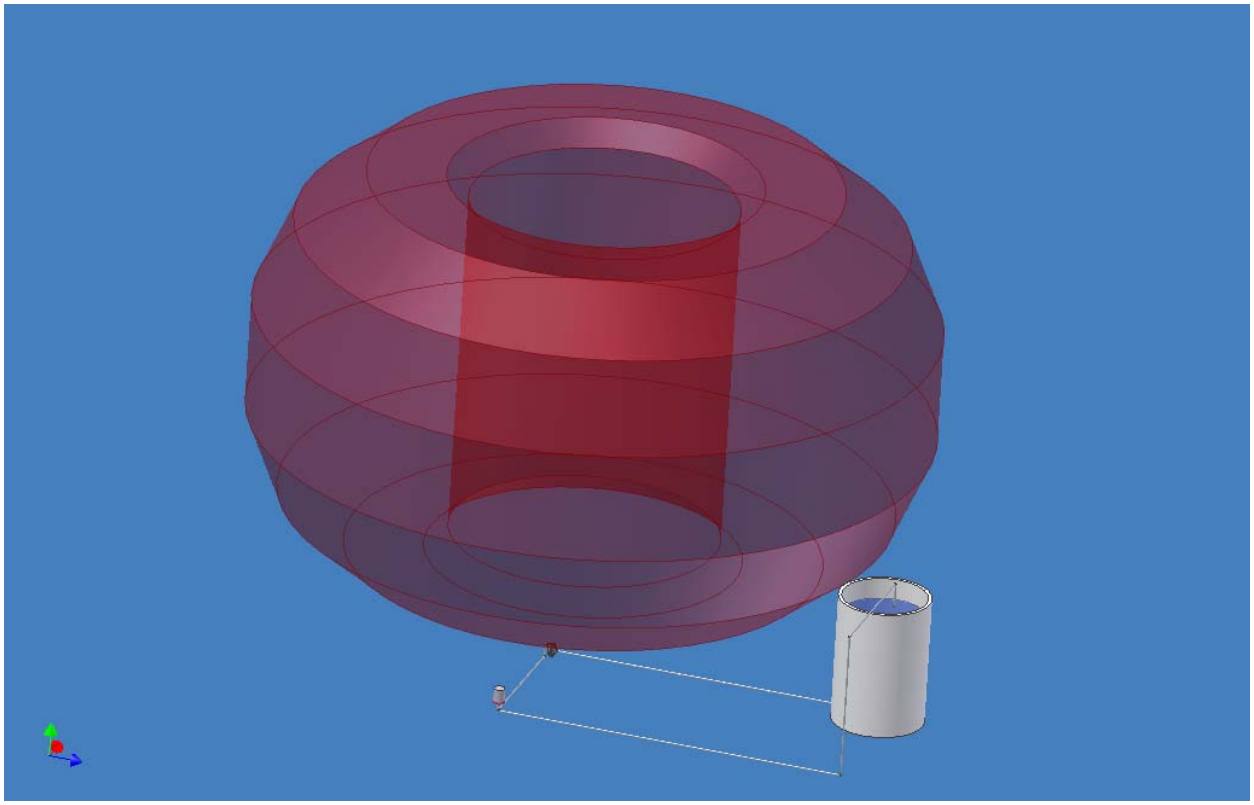

Figure 2.1.1: Power monitoring device. The large, red, translucent structure is the DIII-D vessel

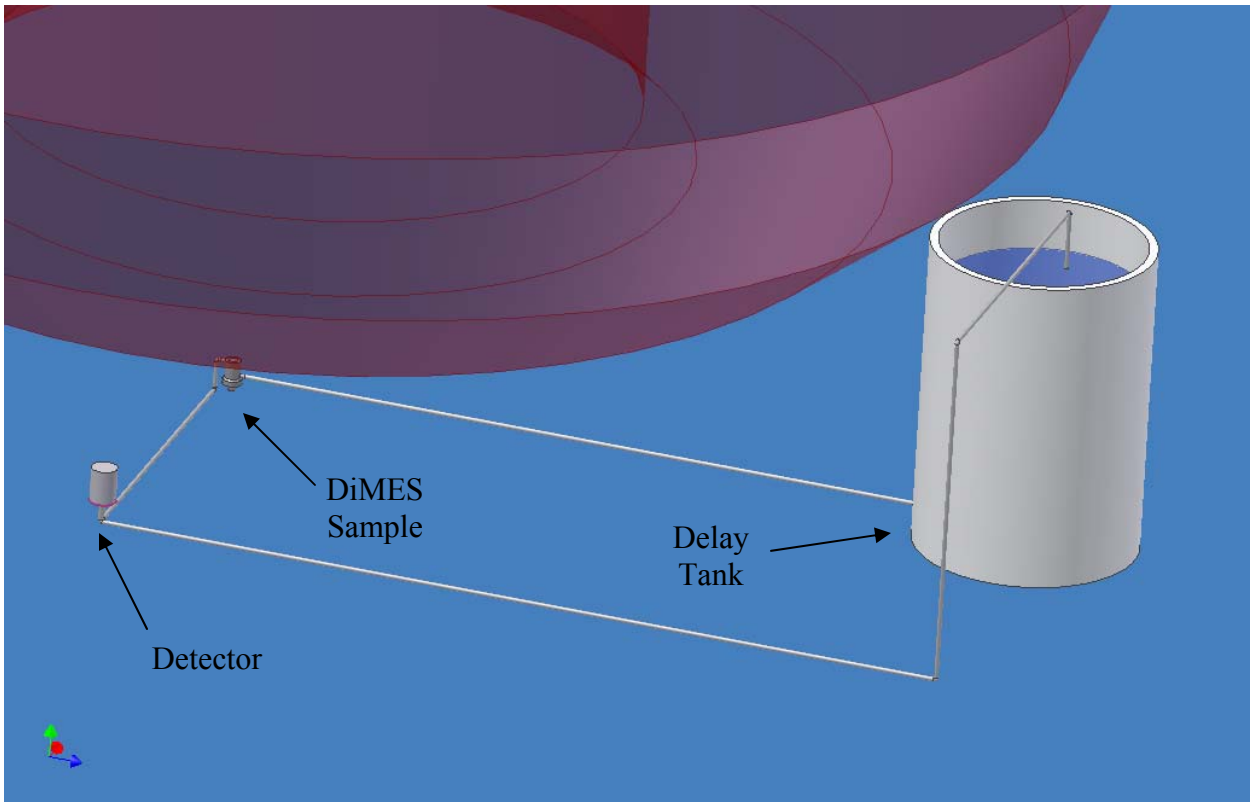

Figure 2.1.2: Power monitoring device. Note that the DiMES sample is located along the bottom of the DIII-D vessel

The DIII-D vessel, as shown in Figure 2.1.1 and Figure 2.1.2 is much larger than the device components. This fact is negligible except when considering the proper modification to the DiMES sample. The placements of the components in Figure 2.1.1 and Figure 2.1.2 are arbitrary, again with the exception of the DiMES sample, which is already predetermined by the size and shape of the installed DiMES device.

Other components will have to be added to the design; mainly a pump, flow-meter, and possibly a heater. These components are removed from Figure 2.1.2 because their presence is supplementary and that their location is customizable.

2.2 Activation Substance

The substance to be activated is chosen based on a given fusion neutron energy. As will be shown later, for D-T the 14.1MeV neutrons make water an ideal activation substance. For D-D, the 2.45MeV neutrons eliminate water as a choice due to the fact that the threshold energy of the (n,p) reaction of ^{16}O is much larger than this neutron energy. Instead, it is necessary to find another substance that is either liquid, or highly soluble in water. If a soluble substance is chosen, it is desired that the solubility be large enough so that a sufficient amount of substance can be injected into the water. To increase solubility, it is easily possible to add a heating element to the design.

Another feature of interest is the neutron capture cross-section. For counting statistics purposes, it is desired for the substance to have a high cross-section value at 2.45MeV for D-D and 14.1MeV for D-T. It would also be desirable for the material to have a relatively smaller cross-section for neutrons of energies below 2.45MeV (or 14.1MeV for D-T), since these neutrons would decrease the resolution of the detector. Of practical importance is the substance's half-life. A value between three and thirty seconds is desired, since any larger values would require a very large delay tank to ensure sufficient decay and any smaller values would imply relatively large amounts of decay before reaching the detector. Finally, it is desired that the activation substance be such that the fluid allow for beta attenuation. The fluid attenuation effects are simulated in MCNP5.

2.3 Delay Tank

The delay tank is sized according to the activation substance's half-life. It is best that ten to twenty half-lives transpire while the fluid is within the delay tank to insure sufficient decay. Volumetric flow rate is conserved between the delay tank and piping, thus

$$v_T A_T = v_P A_P \qquad \text{(Eq. 2.3.1)}$$

where "T" is subscript for delay tank and "P" is subscript for pipe. Optimum pipe velocity and pipe cross-sectional area depend on the flow regime, and are best determined experimentally. For this analysis the JAERI values of $v_P \cong 12\frac{m}{s}$ and $A_P \cong \pi\left(\frac{0.44in}{2}\right)^2 \cong 0.000098099\,m^2$ were adopted for use.[13]. The velocity in the tank is given by

$$v_T = \frac{H_T}{t_T} \qquad \text{(Eq. 2.3.2)}$$

where H_T is the tank height in meters and t_T is the travel time of the activation substance through the delay tank in seconds. The expression is simplified by inserting Equation 2.3.2 into Equation 2.3.1 and solving for tank height.

$$H_T = \frac{A_P v_P t_T}{A_T} \qquad \text{(Eq. 2.3.3)}$$

Thus, for a given delay tank diameter, the tank height can be computed.

The delay tank composition should be chemically inert to the activation substance. It should also be able to withstand moderate amounts of radiation. It may be such that the delay tank should also have a relatively high melting temperature so that a heating element can be applied to it. It may be advantageous for the material to also be translucent so that water level can be visually monitored from a safe distance.

2.4 DiMES Modification

The DiMES sample has to be modified in order to allow for a fluid to flow through it. This can be achieved by re-machining the DiMES (made of graphite) to accommodate fluid circulation. The modification must maximize the fluid irradiation volume, so that the fluid is sufficiently activated. The DiMES sample in the DIII-D fusion test reactor is located in a V-1 port at a toroidal radius of approximately 1.48 meters, and the DIII-D fusion can be approximated as a toroidal line source at a toroidal radius of 1.7 meters, thus they are almost vertically aligned [16]. However, as Figure 2.1.1 and Figure 2.1.2 show, the DiMES sample is still quite small compared to the DIII-D vessel. The modification must be sealed so that no fluid will escape the DiMES into the DIII-D vacuum vessel. The modification must also consider materials that are not affected by the strong magnetic fields from the DIII-D toroidal and poloidal field coils.

2.5 Detector

The detector must be sensitive to betas and gammas. A geometry that approaches 4π is best, since this would maximize the detector's yield. The detector should also be shielded with lead bricks to cutoff or minimize the background counts. The detector must also have a good energy resolution and good stability. In order to maximize beta particle count, it is best if the detector were to have a thin shell but a large volume. If the detector is to come in contact with the fluid then the detector shell must be inert to the fluid. Temperature, and temperature gradients, may not be an issue. Various detector geometries are investigated using MCNP5.

2.6 Piping, Material, and Supplemental Components

The JAERI team used a half-inch diameter pipe, with ~0.4 inch inner diameter [13]. This sizing is recommended for this design since it allows for higher level Reynolds numbers at lower volumetric flow rates. This can be seen from the Reynolds number and the fluid velocity equations.

$$\mathrm{Re} = \frac{\rho v L}{\mu} \qquad \text{(Eq. 2.6.1)}$$

$$\left[\dot{V} = vA\right] \Rightarrow \left[v = \frac{\dot{V}}{A}\right] \qquad \text{(Eq. 2.6.2)}$$

At lower cross-sectional areas, the fluid velocity is higher (Eq. 2.6.2), resulting in higher Reynolds numbers (Eq. 2.6.1). Turbulent flow is ideal because as the JAERI research showed, the ^{16}N yield is modeled best as turbulent flow [13]. If the piping diameter is increased beyond half an inch, then the DiMES sample can't accommodate such a design because the sample is small and it is important for the perfect mixing assumption that the fluid flow enters the sample through an inlet nozzle centered at the bottom of the cylindrical side and exits through an identical nozzle centered at the top of the cylindrical side [17]. If the diameters are large, the nozzles may overlap slightly, thus preventing perfect mixing.

It is crucial that the components be comprised of a material that is non-corrosive with silver nitrate, or else covered by a layer which is non-corrosive. Although silver nitrate is corrosive, it can be easily contained by many ordinary plastics or stainless steel 304 (SS-304).

As has been previously mentioned, the device will employ diagnostic equipment and/or equipment that increases the capacity of the system. Typical diagnostic equipment is a flow-meter and a densometer to monitor the system's operation as well as allow data to be obtained for experimental studies. Components that will increase the capacity of the system include a

variable pump and heater, where the variable pump will increase the fluid's velocity and allow for transition between different flow regimes. As will be shown in Section 3.1, a heater will allow for larger quantities of a soluble substance to be dissolved in water. Although it's likely that the DIII-D will heat the fluid during operation as a result of high heat flux deposition on the divertor, and consequently on top of the DiMES sample, additional heat may be advantageous. The location of the heater would be relatively arbitrary, although it is important that the heating element not damage any materials or components. Any supplemental components are not discussed herein, since their use is not related to the computational study in this research, but mostly related to experimental studies not part of this thesis work.

3 Finalized Design Components and Analysis Results

3.1 Activation Substance

At some point in the future DIII-D will burn D-T as the fusion fuel. This transition is deferred until the ongoing research using the D-D scheme is completed. When burning D-T, there will be 14.1MeV neutrons generated additional to the inventory of the radioactive tritium [8]. When this change occurs, it is recommended that the device use water as the activation fluid; specifically, monitoring the gammas emitted by ^{16}N decay, which is produced via $^{16}O(n,p)^{16}N$. The threshold energy for the $^{16}O(n,p)^{16}N$ reaction is 10.4 MeV, which will prevent lower energy neutrons from distorting the temporal resolution by delaying their contributing counts [13]. Essentially the worry over lower energy neutrons is that they will contribute counts to the wrong time bin. This happens because they spend more time in the DIII-D and surrounding environment before entering the activation volume, thus increasing the probability that a time width has passed. The half-life of the ^{16}N nucleus is 7.13 seconds, emitting 6.13 (68.8%) or 7.12 (4.7%) MeV gamma rays [13]. The cross-section of ^{16}O is also acceptable at a neutron energy of 14.1 MeV, the (n,p) cross-section value of ^{16}O is approximately 0.0427 barns [18]. The attenuation effects of water on the gammas will be presented in Section 3.4; the gamma attenuation is roughly the same between water and the other fluid choice. This is expected since photons carry no net charge and fluid densities are roughly the same between the two choices. If water is the activation fluid, material choices are very simple since water is chemically inert with most materials.

For now DIII-D burns D-D, and since water is not an option at 2.45 MeV, other liquids and solutes must be considered. A very good choice is silver nitrate ($AgNO_3$), with the activation of ^{109}Ag to ^{110}Ag being of interest, since the decay properties of ^{110}Ag are appealing to

this application. The half-life is 24.6 seconds, decaying via beta particles and gamma rays. Of specific interest are the 2.89 (94.91%) or 2.23 (4.41%) MeV betas or 0.66 (4.5%) MeV gammas [19]. Unfortunately ^{109}Ag does not have an attractive threshold energy like ^{16}O, but the cross-section value is still reasonable. At a neutron energy of 2.45 MeV, ^{109}Ag has a capture cross-section value of approximately 0.04 barns [18].

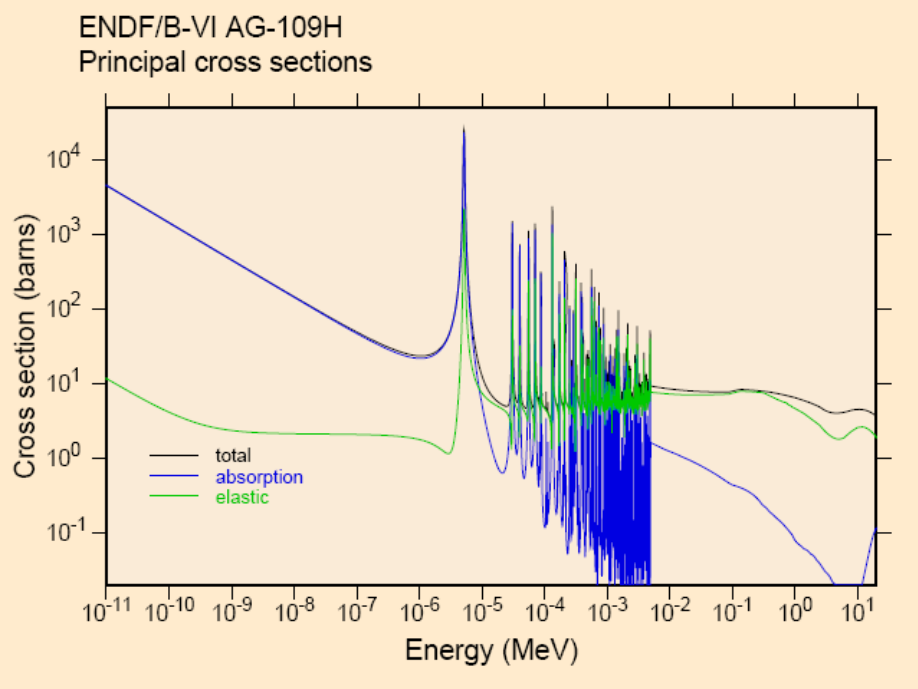

Figure 3.1.1: Cross-section of ^{109}Ag
Taken from Ref. [18] - T-2 Nuclear Information Service. LANL. 6 Dec 2006. <http://t2.lanl.gov/cgi-bin/endlnk?ag109h>

As shown in Figure 3.1.1, lower energy neutrons will contribute to the activation of ^{109}Ag, however, it is postulated that experimental application will show that the effects are negligible at acceptable time widths. Particle attenuation will be discussed in Section 3.4, but it is sufficient to say that beta attenuation is highly dependent upon detector geometry, with acceptable values being achieved. Silver nitrate is also highly soluble in water. The solubility of $AgNO_3$ is shown in Table 3.1.1 [20].

Table 3.1.1: Solubility table of $AgNO_3$ (1 atm, g/100mL)
Taken from Ref. [20] - Salt Lake Metals. 6 Dec 2006.
<http://www.saltlakemetals.com/Solubility_Of_Silver_Nitrate.htm>

0°C	10°C	20°C	30°C	40°C	50°C	60°C	80°C	100°C
122	170	222	300	376	455	525	669	952

The pH and chemical volatility of the silver nitrate will have to be monitored and tested for the device, with special consideration given to material choices. Silver nitrate can be safely contained within plastic, as well as SS-304. However, silver nitrate is poisonous if ingested, thus it should be handled with care and completely sealed within the system. Physical contact with silver nitrate will stain the skin, but not cause health concerns.

3.2 Delay Tank

Applying Equation 2.3.3 yields the following results, as shown in Table 3.2.1.

Table 3.2.1: Delay tank geometry. Note that $t_{1/2}$=24.6 seconds.

T_T ($t_{1/2}$)	D_T (in)	H_T (in)
10	18	34.72
20	18	69.45
10	24	19.53
20	24	39.06
10	36	8.66
20	36	17.32

Interpreting Table 3.2.1 is personal, but it is suggested that the minimum delay tank geometry be a diameter of two feet and height of three feet. This is a standard size that is available, and the necessary number of half-life progressions is likely to be closer to ten than twenty since ten half-lives is the standard for most experimental procedures. Any delay tank

geometry choice based on the decay of ^{110}Ag will be acceptable for water, since the half-life of ^{16}N is significantly less.

The inlet to the delay tank is from the top, while the outlet is via a 0.5 inch hole either through the bottom, or through the bottom of the side. Strong, durable plastics are a good choice for material, as they are chemically inert to $AgNO_3$, and translucent, thus allowing for visual measurement and monitoring of the fluid height. Although not as advantageous due to its lack of translucency, SS-304 is also a good choice, since it easily allows for the addition of a heater. The delay tank can be placed anywhere, however, since it contains activated fluid, it would be safest to either shield the tank or place it at a safe distance from worker personnel. It is also possible that the activated fluid within the tank could add counts to the detector if not properly shielded or kept at a large enough distance from the detector. Beta attenuation is not a major issue, as they can be easily stopped by SS-304 and most plastics.

3.3 DiMES Modification

The irradiation volume can be maximized by hollowing out a cylindrical volume in the sample. This can be done as long as one assumes perfect mixing, implying a uniform radioisotope distribution, and that the density fraction of the radioisotope in the fluid leaving the irradiation volume is at constant proportionality to the density fraction within the irradiation volume. The sample is to be machined in two pieces, a "base" and a "shell." The pieces were designed such that the shell is threaded into the base, enclosing the bottom portion of the shell. A very thin gasket and/or sealant must be added to the interface in order to ensure a tight seal for the circulating fluid not to leak into the DIII-D vessel. The fluid enters the irradiation volume through a half-inch inlet nozzle centered at the bottom of the shell, above the base. The fluid

leaves the irradiation volume through a half-inch exit nozzle centered at the top of the shell, opposite side of the inlet tube. The addition of piping may require holes to be drilled into the DiMES housing and fittings for the piping connections. The modified DiMES components are illustrated in Figure 3.3.1, Figure 3.3.2Figure 3.3.3.

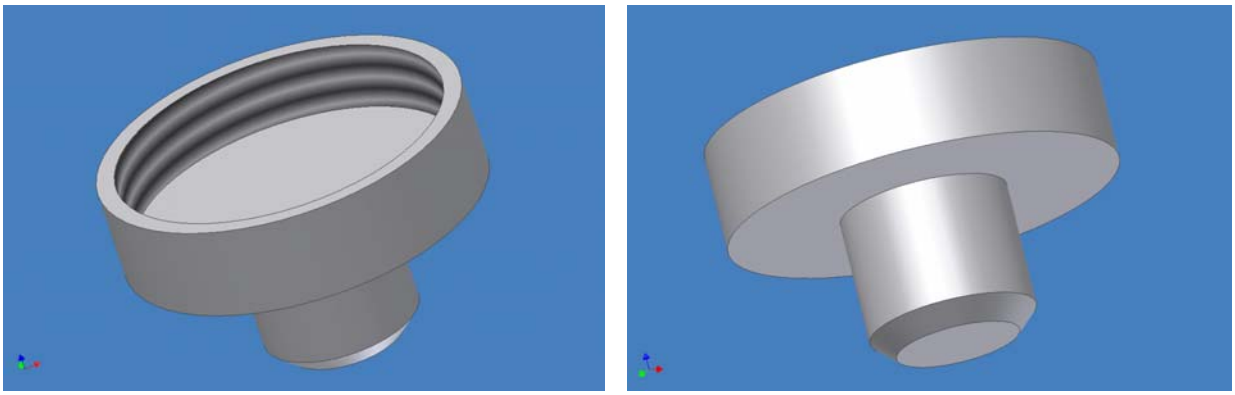

From above From below

Figure 3.3.1: "Base" portion of DiMES modification

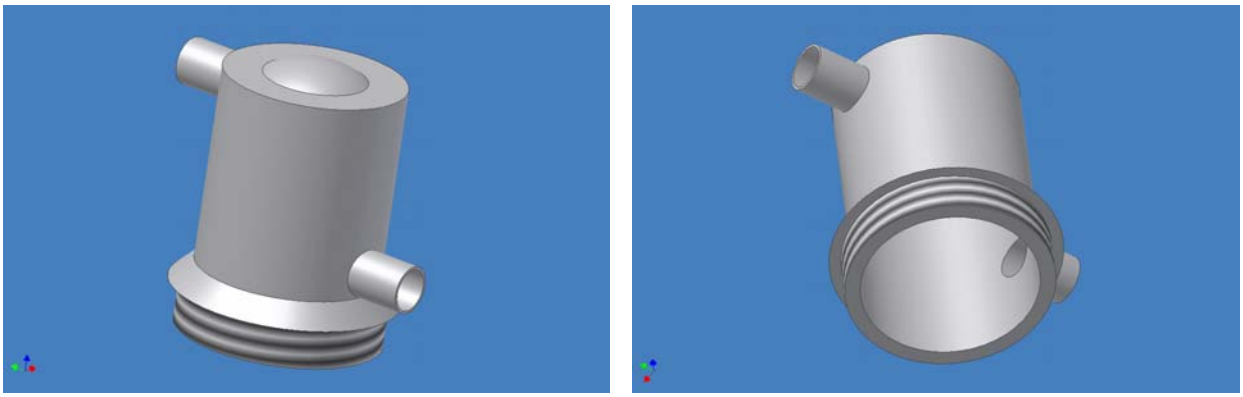

From above From below

Figure 3.3.2: "Shell" portion of DiMES modification

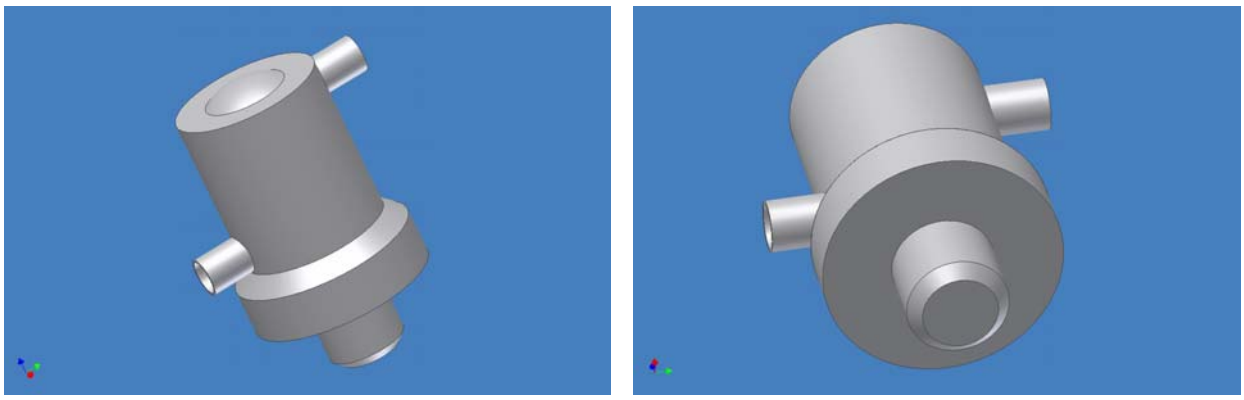

From above From below

Figure 3.3.3: Combined DiMES modification

It is important to notice in Figure 3.3.3 that the outside geometry resembles that of the non-modified DiMES sample, with the exception of the fluid nozzles. This minimizes further modification of the DiMES housing beyond what is necessary for piping.

The geometry was simulated in MCNP5 to evaluate its yield. The input was simplified in that no materials were used and the only components were the DIII-D vessel, DiMES irradiation volume, and DiMES housing. The DIII-D vessel and DiMES housing were both approximated to best knowledge as obtained from General Atomics documentation. If a source particle exited any of these components it was no longer tracked. These simplifications were made for a couple reasons. First, the true geometry and materials of the DIII-D vessel is very complex. Second, it was assumed that making correct limiting assumptions would be better than making incorrect/inaccurate limiting assumptions; if the device would work for a conservative simulation, then it should certainly work for a more detailed simulation. In reality, the simulation input is quite conservative. In an actual experiment, attenuation and scattering would remarkably increase the yield. Instead of looking at tallies, the number of tracks entering the DiMES irradiation volume was used; this is "Counts" in the following Table 3.3.1.

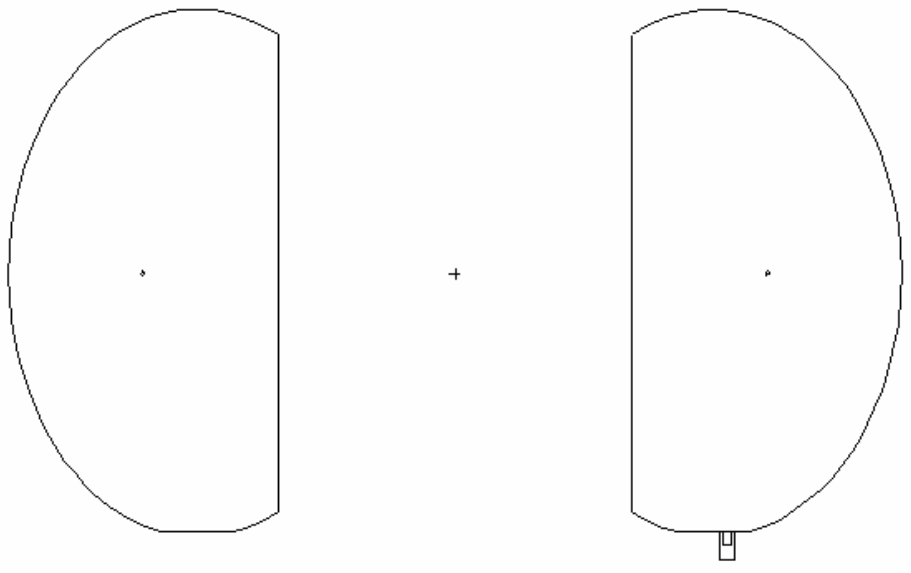

Figure 3.3.4: MCNP5 activation geometry shown in Visual Editor

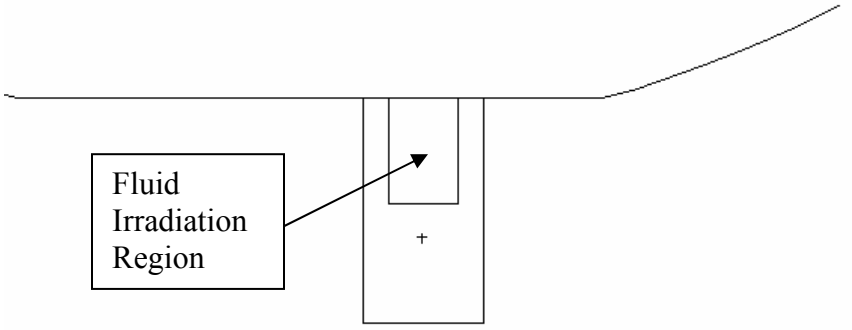

Figure 3.3.5: MCNP5 activation geometry shown in Visual Editor, zoomed in on DiMES

The source region of Figure 3.3.4 is a little difficult to see; it appears as the dot in the middle of the DIII-D vessel, both sides. The source is a torus centered in the DIII-D vessel, and located at a toroidal radius of 1.7 meters. The torus itself has a small radius (1cm) to simulate a pseudo toroidal line source.

The MCNP5 simulation output was used to calculate activation yield. This value can be interpreted as the percent of fusion neutrons that will produce a radionuclide (^{110}Ag or ^{16}N) in the irradiation volume. The yield was calculated as the following product:

$$\frac{\alpha \Sigma V}{A} \qquad \text{(Eq. 3.3.1)}$$

where,

α Count

Σ Macroscopic Cross - section (either capture or (n, p), units of cm^{-1})

V Irradiation Volume (cm^3)

A Surface Area of Irradiation Volume (cm^2)

The results yielded the following values, as shown in Table 3.3.1.

Table 3.3.1: MCNP5 counts and activation yields

	Count	Total Yield
$AgNO_3$	0.002555%	2.015×10^{-7}%
H_2O	0.002555%	3.088×10^{-6}%

For $AgNO_3$:

$$\frac{\Sigma_C V}{A} = \frac{\sigma_C N V}{A} = \frac{\left(0.0398 x 10^{-24} cm^2\right)\left(2.3406 x 10^{21} cm^{-3}\right)\left(102.963 cm^3\right)}{121.6098 cm^2} = 7.8872 x 10^{-5}$$

For H_2O:

$$\frac{\Sigma_{(n,p)} V}{A} = \frac{\sigma_{(n,p)} N V}{A} = \frac{\left(0.0427 x 10^{-24} cm^2\right)\left(3.3428 x 10^{22} cm^{-3}\right)\left(102.963 cm^3\right)}{121.6098 cm^2} = 0.0012085$$

Thus if water were used as the activation fluid, yields would increase by an order of magnitude. However, this does not mean that $AgNO_3$ yields are too small; the yield is simply factored into the real-time power program (Chapter 4).

3.4 Detector and Detection Geometry

A suitable detector choice is a sodium iodide crystal with thallium integrated into the crystal structure. Abbreviated by NaI(Tl), this alkali halide scintillation detector exhibits extremely good light yield and excellent linearity [21]. The detector works by emitting light that is proportional to the incident radiation. This light originates from a unique property of the crystal structure. For some inorganic crystals (e.g. NaI) electrons can only exist in discrete bands of energy. The lower band is referred to as the valence band, and represents those electrons which are essentially bound at lattice sites [21]. The upper band is referred to as the conduction band and represents those electrons that have sufficient energy to free themselves and migrate throughout the crystal [21]. No electrons can exist between the valance and conduction bands, but when energy absorption by the crystal raises an electron from the valance band into the conduction band, a hole is formed in the normally filled valence band. The return of an electron to fill this hole is accompanied by the emission of a photon. With the addition of an activator (e.g. thallium) the probability of the photon being within visible light range increases. Once the visible light is generated it is then manipulated by a photomultiplier tube, which increases the intensity, then counted by a photodiode (i.e. converted into a proportional electrical pulse). Although most commonly used for gamma spectroscopy, NaI(Tl) detectors are also sensitive to beta particles.

NaI crystals can be formed into unusual sizes and shapes by pressing small crystallites together [21]. This allows for much freedom while investigating detector geometries. A variety of NaI(Tl) detectors are available in the market and can be purchased from different manufacturers/vendors (e.g. Saint-Gobain <http://www.detectors.saint-gobain.com>), but this research narrowed the choices down to two detectors and three geometries. The three geometries

were simulated in MCNP5 in order to determine which geometry produced the largest detector yield. The F8 tally was employed, which simulates a detector response. Simulations were carried out for both H_2O and $AgNO_3$, where perfect mixing is assumed, resulting in uniform radionuclide distribution. The $AgNO_3$ simulations investigated three different detection modes: detecting just the 0.66 (4.5%) MeV gammas, just the 2.89 (94.91%) betas, or both the 2.89 (94.91%) and 2.23 (4.41%) MeV beta particles. The H_2O simulations looked at detecting both the 6.13 (68.8%) and 7.12 (4.7%) gamma rays. The first detector was comprised of a typical cylindrically shaped NaI crystal (2 inch diameter by 2 inch height, abbreviated by 2"X2"). The second detector was also comprised of a cylindrically shaped NaI crystal (3"X4"), but this time it had a well penetrating into it from the bottom (1.25"X3") [22].

The first simulation geometry employed the 2"X2" crystal, where the detector is in the center of a concentric cylindrical tank containing the irradiated fluid. The fluid tank has an outer diameter of 2.93 inches, inner diameter of 2.14 inches, and a height of 2.1 inches.

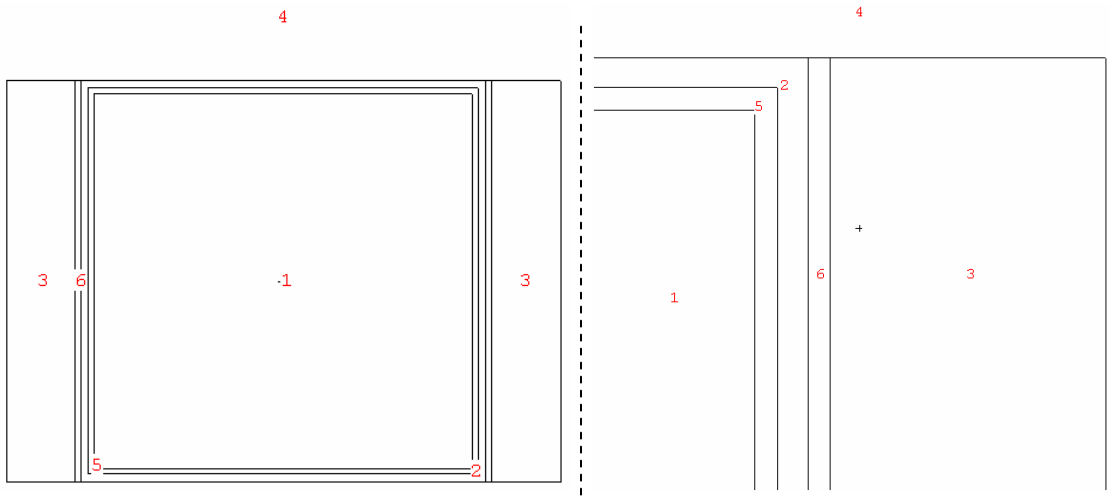

Complete Zoomed (upper-right)

Figure 3.4.1: MCNP5 geometry 1 shown in Visual Editor

It should be noted in Figure 3.4.1 that the cells are numbered, where

Cell 1: NaI crystal
Cell 2: Gap
Cell 3: Irradiated fluid region
Cell 4: Ambient
Cell 5: Detector lining (Al)
Cell 6: Fluid container lining (SS-304)

The advantages of a geometry such as the one shown in Figure 3.4.1 is that the detector can be easily removed from the setup for maintenance or repair and that the fluid is easily isolated and contained. The disadvantage is that validating a perfect mixing assumption for such a geometry would be difficult and also a smaller fraction of radiation is detected when compared with other geometries, thus resulting in a lower yield.

The second simulation geometry also employed the 2"X2" crystal, where the detector is partially dipped into a tank containing the irradiated fluid, again all shapes are cylindrical. The fluid contained within the tank has both a diameter and height of 2.25 inches when the detector is dipped a distance of 0.75 inches.

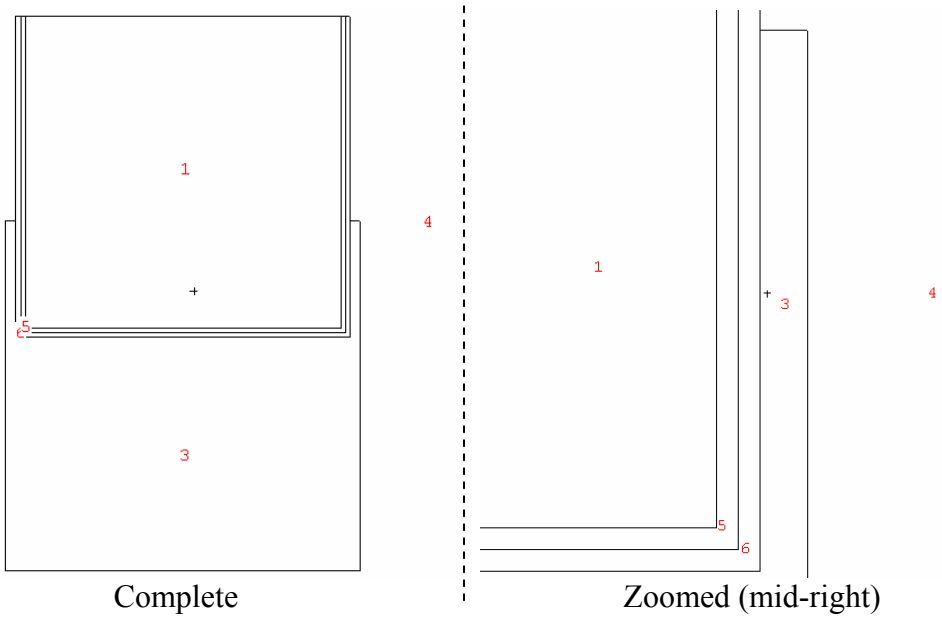

Complete Zoomed (mid-right)

Figure 3.4.2: MCNP5 geometry 2 shown in Visual Editor

Where the numbering on Figure 3.4.2 is for the cells as indicated below:

Cell 1: NaI crystal
Cell 2: Gap (too small to show)
Cell 3: Irradiated fluid region
Cell 4: Ambient
Cell 5: Detector lining (Al)
Cell 6: Additional detector lining (SS-304)

The advantage of such a geometry as in Figure 3.4.2 is that obtaining a perfect mixing assumption is easier. The disadvantage of such a geometry is that one must be careful when dipping the detector into the tank. An inert layer, such as SS-304 must cover the detector, and such a layer would mitigate beta attenuation.

The third simulation geometry, and most unique, employed the well design, where again all shapes are cylindrical. The irradiated fluid is circulated in the well. The MCNP geometry for this simulation is shown in Figure 3.4.3.

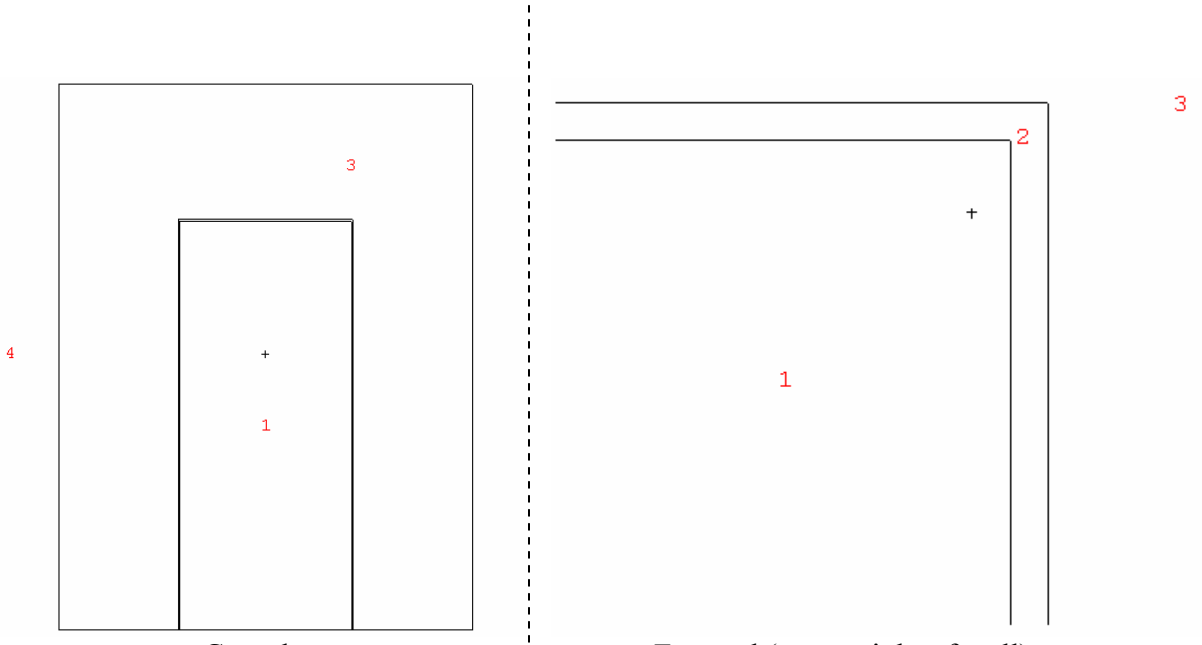

Complete Zoomed (upper-right of well)

Figure 3.4.3: MCNP geometry 3 shown in Visual Editor

Where once more it should be noted about Figure 3.4.3 that

Cell 1: Irradiated fluid region
Cell 2: Well lining (Al)Gap (too small to show)
Cell 3: NaI crystal
Cell 4: Ambient

The irradiated fluid enters the well through the bottom, on one side, and exit on the other, having great advantage on containing the fluid almost completely within the NaI crystal, thus producing a near 4π geometry and a higher detection yield. The well is also lined with 0.01 inch thick aluminum, instead of the mirror, aluminum, and mechanical shock absorber (i.e. sponge) that normally lines the exterior of the crystal, thus increasing attenuation. The only disadvantage is that the well is relatively of small volume, which makes it difficult to validate perfect mixing.

The MCNP5 simulation output was used to calculate detection yield, which is then interpreted as the percent of pertinent radiation emitted by the fluid that will be detected. The yield is the product of the tally and the decay occurrence:

$$\beta\gamma \qquad \text{(Eq. 3.4.1)}$$

The resulting detection yields of $AgNO_3$ are shown in Table 3.4.1, and that for water are shown in Table 3.4.2.

Table 3.4.1: MCNP5 tallies and detection yields ($AgNO_3$)

	Tally	Total Yield
	Detection Geometry 1	
Gamma (1)	24.09%	1.08%
Beta (2)	1.46%	1.45%
Beta (1)	1.70%	1.61%
	Detection Geometry 2	
Gamma (1)	15.13%	0.68%
Beta (2)	1.18%	1.17%
Beta (1)	1.17%	1.11%
	Detection Geometry 3	
Gamma (1)	92.67%	4.17%
Beta (2)	65.51%	65.06%
Beta (1)	64.34%	61.07%

Table 3.4.2: MCNP5 tallies and detection yields (H_2O)

	Tally	Total Yield
	Detection Geometry 1	
Gamma (2)	24.05%	17.80%
	Detection Geometry 2	
Gamma (2)	16.40%	12.13%
	Detection Geometry 3	
Gamma (2)	94.36%	69.83%

As seen from the results in Table 3.4.1 and Table 3.4.2, the maximum yield for both activation fluids was achieved in detection geometry three. This is expected due to the fact that the crystal in detection geometry three almost completely surrounds the irradiated fluid, which is a near 4π setup. Thus, as Table 3.4.1 and Table 3.4.2 indicate, the best setup with $AgNO_3$ as the activation fluid would be the detection geometry three, where both beta particles are being recorded. If the activation fluid were H_2O, then detection geometry three is still the best at detecting both gammas.

4 Real-time Power Monitoring

4.1 Mathematical Overview

In order to develop the design into a real-time application, a mathematical understanding of the underlying processes must be understood. Counts, and thus count-rates, will be recorded at regular time intervals. The population density $N_D(t)$ of radionuclides in the detection volume has unites of (#/cm^3) and can be computed using the following relation:

$$N_D(t) = \frac{C(t)}{V_D \lambda \beta \gamma} \qquad \text{(Eq. 4.1.1)}$$

where,

$C(t)$ Count - rate (#/s)
V_D Detection Volume (cm^3)
λ Radionuclide Decay Constant (s^{-1})
$\beta\gamma$ Detection Yield (dimensionless)

Once counting is completed then one calculates the population density of radionuclides in the activation volume. This requires the solution of Eq. 4.1.2.

$$V_D \frac{dN_D(t)}{dt} = QN_A(t-\tau)e^{-\lambda\tau} - \lambda V_D N_D(t) - QN_D(t) \qquad \text{(Eq. 4.1.2)}$$

Where $QN_A(t-\tau)e^{-\lambda\tau}$ is the mass flow-rate from the activation volume and arrival rate in the detection volume without decay. The term $\lambda V_D N_D(t)$ is the loss by decay in the detection volume and $QN_D(t)$ is the radionuclide mass flow-rate from the detection volume. The above equations can be algebraically rearranged to calculate the population density of radionuclides in the activation volume.

$$N_A(t-\tau) = \frac{V_D\left(\frac{dN_D(t)}{dt}\right) + \lambda V_D N_D(t) + QN_D(t)}{Qe^{-\lambda\tau}} \qquad \text{(Eq. 4.1.3)}$$

where,

Q Volumetric Flow - rate (cm^3/s)

τ Elapsed Time Between Activation and Detection Volumes (s)

The presence of τ implies that the device is not truly real-time, it is partially delayed by the τ value, which is dependent upon the flow velocity. This implies that the device is not suitable for reactor control.

Unfortunately the shape of $N_D(t)$ is not known, thus to calculate its derivative with respect to time involves a numerical derivative technique; the one employed is the "five-point formula," as shown in Eq. 4.1.4 [23].

$$\frac{dN_D(t)}{dt} = \frac{1}{12\Delta t}[N_D(t-2\Delta t) - 8N_D(t-\Delta t) + 8N_D(t+\Delta t) - N_D(t+2\Delta t)] \qquad \text{(Eq. 4.1.4)}$$

The five-point formula is derived in Appendix II. Employing Equation 4.1.4 means that the power values can not be accurately calculated for the first and last two timestamps. This is because they do not have all four extension values: $N_D(t-2\Delta t)$, $N_D(t-\Delta t)$, $N_D(t+\Delta t)$, or $N_D(t+2\Delta)$. The five-point formula also contributes to delaying the power computation by two time intervals, since both $N_D(t+\Delta t)$ and $N_D(t+2\Delta t)$ values are needed. Also important to note is that the five-point formula introduces error of the form

$$\frac{\varepsilon}{\Delta t} + \frac{(\Delta t)^4 f^{(5)}(x)}{30}$$

where ε represents the precision (roundoff) of the numerical calculation [23]. It is interesting to note that to reduce the truncation error (second term), one must reduce Δt, yet reducing Δt will

increase the roundoff error (first term). The functional form of the behavior is unknown for this application, thus truncation error can not be explicitly calculated. The program employs double precision, which doubles the bit storage for each number, thus making roundoff error completely negligible.

The next step is to calculate the production rate of radionuclides from Eq. 4.1.5.

$$V_A \frac{dN_A(t-\tau)}{dt} = R(t-\tau) - \lambda V_A N_A(t-\tau) - QN_A(t-\tau) \qquad \text{(Eq. 4.1.5)}$$

Where $R(t-\tau)$ is the radionuclide's production rate, units of (#/s). Term $\lambda V_A N_A(t-\tau)$ is the loss by decay in the activation volume and $QN_A(t-\tau)$ is the radionuclide mass flow-rate from the activation volume. This equation can be rearranged to calculate the radionuclide production rate.

$$R(t-\tau) = V_A \frac{dN_A(t-\tau)}{dt} + \lambda V_A N_A(t-\tau) + QN_A(t-\tau) \qquad \text{(Eq. 4.1.6)}$$

The five-point formula is also employed to numerically calculate the derivative $\frac{dN_A(t-\tau)}{dt}$. This implies that the first and last four power calculations will be inaccurate, since the number of time intervals needed is two intervals in each direction (i.e. history and future). These erroneous data points will not cause distress if the device begins recording at least five time intervals before power calculations are needed and stops recording at least five time intervals after power calculations are needed.

The next step is to calculate the neutron activity, with units (#/s), of the fusion source. This value can be obtained from Eq. 4.1.7.

$$A(t-\tau) = \frac{R(t-\tau)A}{\alpha \Sigma V} \qquad \text{(Eq. 4.1.7)}$$

where, $\frac{A}{\alpha \Sigma V}$ is the inverse of the activation yield.

Once activity is calculated, the final step is to calculate the fusion power as

$$P_{fus}(t-\tau) = A(t-\tau)E \qquad \text{(Eq. 4.1.8)}$$

where E is the emission energy of the fusion neutron. Watt is the unit for power, assume the unit for energy release is a joule.

As has mathematically been shown, one can compute the fusion power by employing five equations in series: Equations 4.1.1 through 4.1.8. The solution flow diagram appears as

$$C(t) \rightarrow N_D(t) \rightarrow \frac{dN_D(t)}{dt} \rightarrow N_A(t-\tau) \rightarrow \frac{dN_A(t-\tau)}{dt} \rightarrow R(t-\tau) \rightarrow A(t-\tau) \rightarrow P_{fus}(t-\tau)$$

4.2 "Count-to-Power" FORTRAN Program

Equations in Section 4.1 were employed to write a FORTRAN-95 program, named "Count-to-Power" or abbreviated as C2P, to calculate the fusion power from detector counts. Documentation of the C2P program is in Appendix I. Variables are changed via an input file, and a steady-state option is available, in which the derivatives of Equations 4.1.3 and 4.1.6 are set to zero.

There is no current experimental data to benchmark the program. However, future work in which an actual device would be built would allow for benchmarking. The C2P program can also be applied to any radiation source with circulating fluid being activated and counted.

Test-runs to investigate the behavior of the program have been executed for both $AgNO_3$ and H_2O. All test runs in this section were performed assuming the use of $AgNO_3$ fluid. The first test-run assumed a simple linear increase in count-rate for a relatively small number of time

intervals. The output is shown in Table 4.2.1 and graphically shown in Figure 4.2.1, where the input variables are given in Table 4.2.2.

Table 4.2.1: C2P linear run

Time (s)	Count-rate (s^{-1})	Power (W)	Δ Power (W)
0.25	500	N/A	-
0.5	850	N/A	-
0.75	1200	N/A	-
1	1550	N/A	-
1.25	1900	445.60	-
1.5	2250	519.50	73.91
1.75	2600	593.41	73.91
2	2950	667.32	73.91
2.25	3300	741.23	73.91
2.5	3650	815.14	73.91
2.75	4000	889.05	73.91
3	4350	962.96	73.91
3.25	4700	1036.87	73.91
3.5	5050	1110.78	73.91
3.75	5400	1184.69	73.91
4	5750	1258.60	73.91
4.25	6100	1332.51	73.91
4.5	6450	1406.42	73.91
4.75	6800	1480.33	73.91
5	7150	1554.24	73.91
5.25	7500	N/A	-
5.5	7850	N/A	-
5.75	8200	N/A	-
6	8550	N/A	-

Table 4.2.2: C2P linear run input

Input	Value
V_D	$0.00006033m^3$
V_A	$0.000116767m^3$
λ	$0.0281767s^{-1}$
Y_D	0.6506
Q	$0.0011772m^3/s$
tau	0.75 sec
Y_A	2.01518E-09
E	2.45 MeV

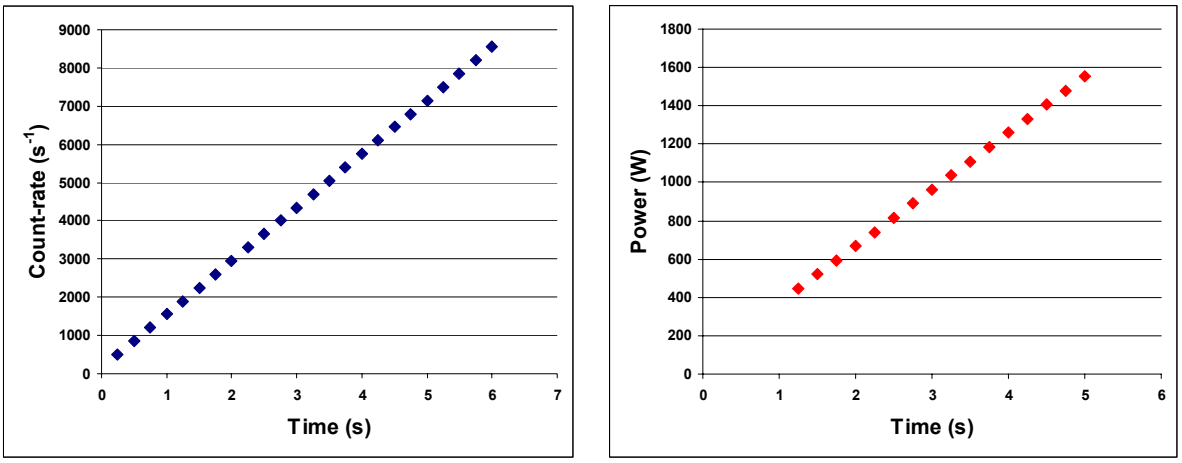

Input Output

Figure 4.2.1: C2P linear run

It is evident from Figure 4.2.1 that a linear increase in count-rate produces a near linear increase in power and Table 4.2.1 shows the numerical values for the "Δ Power (W)."

The neutron activity at the DiMES location during a fusion shot in the DIII-D tokamak is generally plateau shaped [10]. As a result, the expected count-rate trend will take a logarithmic shape during the time associated with activation and an inverse exponential shape during the decay time. The degree of curvature is dependent upon how quickly the fluid is circulated through the irradiation volume. A slower circulation through the activation volume will result in a more 'gradual' curve, where faster circulation will result in a more 'sharp' behavior. The device has a very small activation volume (~0.0001168m^3), with an expected high fluid velocity (~12m/s through 0.44 inch pipes), which means one can most likely expect count-rate behavior of the latter kind (i.e. sharp curvature). Both behaviors were simulated in the C2P program. On the sharp end of the spectrum, the count-rates versus power as calculated by the C2P program are shown in Table 4.2.3, and shown graphically in Figure 4.2.2, with the input variables as given in Table 4.2.2.

Table 4.2.3: C2P sharp run

Time (s)	Count-rate (s^{-1})	Power (W)
0.25	1	N/A
0.5	2	N/A
0.75	3	N/A
1	25	N/A
1.25	800	455.99
1.5	4000	1544.85
1.75	10000	2475.43
2	10000	2033.28
2.25	10000	2137.01
2.5	10000	2125.91
2.75	10000	2126.63
3	10000	2126.63
3.25	10000	2126.63
3.5	10000	2126.63
3.75	10000	2126.63
4	10000	2126.63
4.25	10000	2126.63
4.5	10000	2126.03
4.75	10000	2135.12
5	10000	2157.66
5.25	10000	1734.99
5.5	5000	402.75
5.75	1000	5.46
6	700	N/A
6.25	400	N/A
6.5	200	N/A
6.75	80	N/A

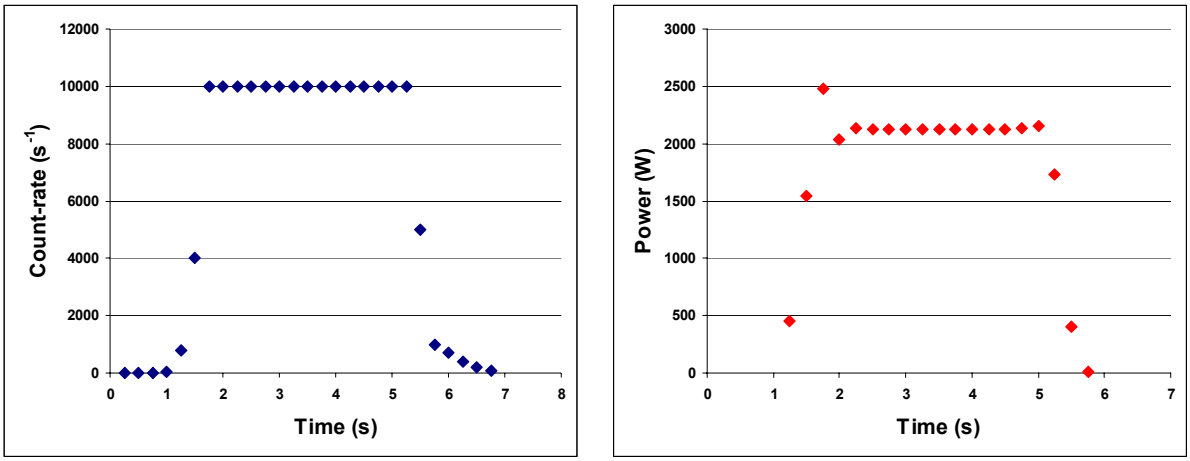

Input Output

Figure 4.2.2: C2P sharp run

The count-rate behavior in Figure 4.2.2 (Input) is highly dramatized. Although the expected behavior is a sharp curvature, it is still not expected to form such a highly distinctive plateau. The input was generated in such a way as to test the C2P program on how well it handles disjoint behavior, which is seen as the transitions to and from the plateau of Figure 4.2.2 (Input). Indeed, as Figure 4.2.2 (Output) reveals, the result is an inaccurate estimate of power. Although the general plateau shape is conserved, the transition behavior skews a few power estimates. This is a consequence of the five-point formula and a weakness of numerical derivative techniques. Fortunately, the experimental count-rate behavior is not expected to take such an exaggerated sharp curvature.

On the lethargic end of the spectrum, the count-rates versus power as calculated by the C2P program are shown in Table 4.2.4, and shown graphically in Figure 4.2.3, with the input variables held unchanged as previously given in Table 4.2.2.

Table 4.2.4: C2P lethargic run

Time (s)	Count-rate (s^{-1})	Power (W)
0.25	2	N/A
0.5	1	N/A
0.75	3	N/A
1	25	N/A
1.25	1562	532.56
1.5	2838	746.22
1.75	3917	958.39
2	4852	1141.72
2.25	5677	1305.08
2.5	6414	1452.12
2.75	7081	1586.10
3	7690	1709.07
3.25	8251	1822.70
3.5	8769	1928.00
3.75	9252	2026.64
4	9704	2119.05
4.25	10128	2206.05
4.5	10529	2288.39
4.75	10907	2366.39

Table 4.2.4 (continued)

Time (s)	Count-rate (s^{-1})	Power (W)
5	11266	2446.71
5.25	11608	2502.28
5.5	11614	2266.13
5.75	9045	1597.58
6	7044	1286.14
6.25	5486	997.15
6.5	4273	776.99
6.75	3328	605.13
7	2592	471.24
7.25	2018	366.90
7.5	1572	285.85
7.75	1224	222.50
8	953	173.25
8.25	742	N/A
8.5	578	N/A
8.75	450	N/A
9	351	N/A

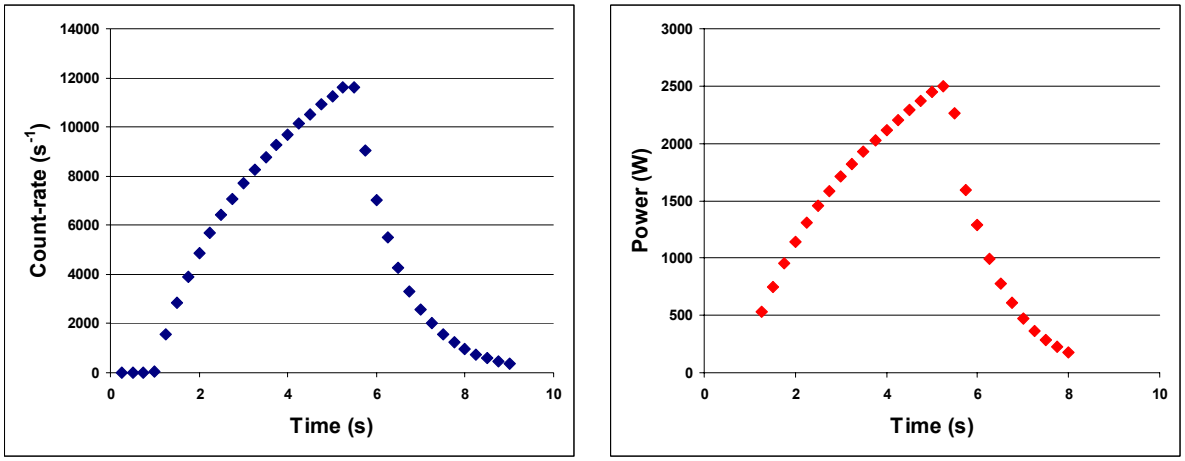

Input Output

Figure 4.2.3: C2P lethargic run

More timestamps were used for the lethargic run than the sharp run so that the activated fluid could be completely circulated out of the detection volume (i.e. count-rate approaches zero). The lethargic input reveals a matching behavior between count-rate and power.

4.3 C2P Behavioral Analysis – $AgNO_3$

Main input variables are fixed for each run. That is, the activation and detection geometries are fixed and non-adjustable, activation substance is constant, and prompt fusion neutron energy is constant. However, both volumetric flow-rate and τ can be adjusted by changing the fluid's velocity via a pump. The behavioral dependence on these two variables was investigated for both $AgNO_3$ fluid and H_2O, with $AgNO_3$ presented here, in Section 4.3. The lethargic input was chosen as the subject since it is more easily treatable by the five-point formula, and more closely models what is experimentally expected, since the sharp input is very extreme.

The volumetric flow-rate was investigated for the case where the pipe has a diameter of 0.44 inches, and a flow velocity of 12m/s. The volumetric flow-rate value was increased to an equivalent of a one inch diameter pipe with constant 12m/s velocity (or this may be seen as fluid velocity increasing to 61.98m/s with a constant 0.44 inch diameter pipe). Such a high fluid velocity is unlikely, but increasing the pipe diameter to one inch is applicable. The volumetric flow-rate was then decreased to an equivalent of a 0.21 inch diameter pipe with constant 12m/s velocity (or a fluid velocity of 2.73 m/s with the original 0.44 inch diameter pipe). The results are shown in Table 4.3.1, and the input values are shown in Table 4.3.2. The power behavior as a function of time for increased and decreased Q is shown in Figure 4.3.1.

Table 4.3.1: C2P Q Investigation ($AgNO_3$)

	Diameter (in)------	0.44	1	0.21
	v (m/s)----------	12.00	61.98	2.73
	Q (m^3/s)----------	0.0011772	0.0060805	0.00026815
Time (s)	**Count-rate (s^{-1})**	**Power (W)**		
0.25	2	N/A	N/A	N/A
0.5	1	N/A	N/A	N/A
0.75	3	N/A	N/A	N/A
1	25	N/A	N/A	N/A

Table 4.3.1 (continued)

Time (s)	Count-rate (s^{-1})	Power (W)		
1.25	1562	532.56	1907.92	287.19
1.5	2838	746.22	3254.40	261.35
1.75	3917	958.39	4414.98	311.06
2	4852	1141.72	5422.74	342.65
2.25	5677	1305.08	6313.49	372.31
2.5	6414	1452.12	7110.38	399.76
2.75	7081	1586.10	7832.52	425.37
3	7690	1709.07	8492.55	449.22
3.25	8251	1822.70	9100.92	471.44
3.5	8769	1928.00	9663.04	492.40
3.75	9252	2026.64	10187.64	512.29
4	9704	2119.05	10678.69	530.97
4.25	10128	2206.05	11139.64	548.82
4.5	10529	2288.39	11575.69	565.54
4.75	10907	2366.39	11986.86	582.78
5	11266	2446.71	12381.54	613.99
5.25	11608	2502.28	12753.66	551.05
5.5	11614	2266.13	12535.05	262.44
5.75	9045	1597.58	9577.86	109.23
6	7044	1286.14	7489.15	176.79
6.25	5486	997.15	5831.87	117.62
6.5	4273	776.99	4542.47	92.95
6.75	3328	605.13	3537.86	72.35
7	2592	471.24	2755.38	56.30
7.25	2018	366.90	2145.21	43.88
7.5	1572	285.85	1671.14	34.19
7.75	1224	222.50	1301.12	26.55
8	953	173.25	1013.05	20.71
8.25	742	N/A	N/A	N/A
8.5	578	N/A	N/A	N/A
8.75	450	N/A	N/A	N/A
9	351	N/A	N/A	N/A

Table 4.3.2: C2P Q investigation input ($AgNO_3$)

Input	Value
V_D	$0.00006033m^3$
V_A	$0.000116767m^3$
Λ	$0.0281767s^{-1}$
Y_D	0.6506
Q	Variable
Tau	0.75 sec
Y_A	2.01518E-09
E	2.45 MeV

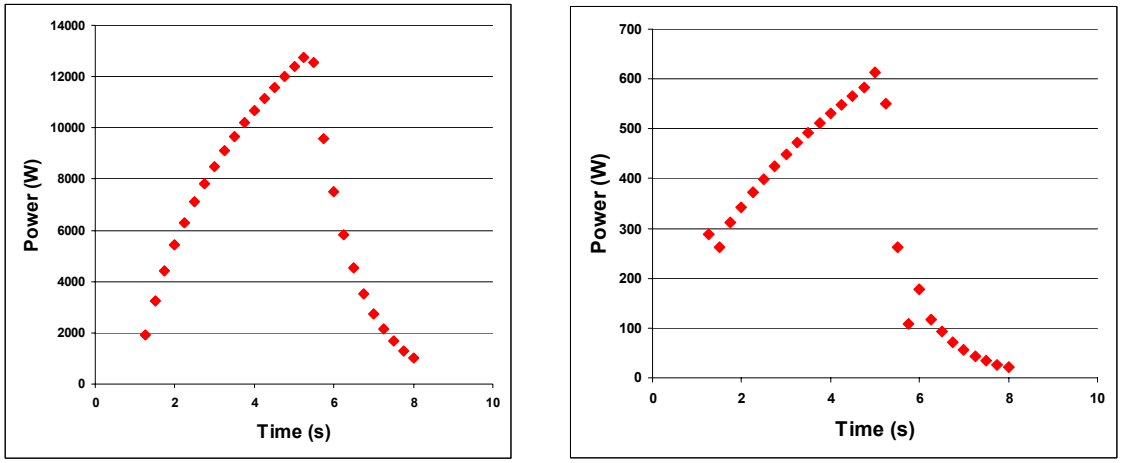

Increase Decrease

Figure 4.3.1: C2P Q investigation ($AgNO_3$)

As shown in Figure 4.3.1, increasing the volumetric flow-rate scaled the power values by approximately a factor of four, without noticeable change in the power shape. Decreasing the volumetric flow-rate did produce a noticeable change in the power shape, as well as scaling down the power values. The ascending (activation) portion of the power response in Figure 4.3.1 (Decrease) appears more linear than logarithmic. The volumetric flow-rate appears as a constant multiple of the exponential term in Equations 4.1.2 and 4.1.3, thus it is clear that as Q significantly decreases, the nonlinear effects of the model equation will be weakened. It is interesting to note that Figure 4.3.1 more closely resembles what is expected of an experimental run of the DIII-D tokamak fusion experimental reactor, in which the power approaches the "resemblance" of a plateau shape during the five second activation period.

Next is to investigate the transport delay value, τ. In the previous computational runs it was assumed that the value of τ was 0.75 seconds. For a 12m/s fluid flow, this corresponds to a pipe length of 9 meters (roughly 29.5 feet). The value of τ was first increased by a factor of four (3.0 seconds), corresponding to an increase in pipe length by a factor of four, or a decrease in

flow velocity by a factor of four. The effect on the computed power when changing τ is shown in Table 4.3.3 and graphically in Figure 4.3.2. All input values for these calculations are given in Table 4.3.4.

Table 4.3.3: C2P τ investigation ($AgNO_3$)

	Tau (s)----------	0.75	3	0.2
Time (s)	**Count-rate (s^{-1})**	**Power (W)**		
0.25	2	N/A	N/A	N/A
0.5	1	N/A	N/A	N/A
0.75	3	N/A	N/A	N/A
1	25	N/A	N/A	N/A
1.25	1562	532.56	567.41	524.37
1.5	2838	746.22	795.06	734.74
1.75	3917	958.39	1021.12	943.65
2	4852	1141.72	1216.45	1124.16
2.25	5677	1305.08	1390.50	1285.01
2.5	6414	1452.12	1547.16	1429.79
2.75	7081	1586.10	1689.91	1561.71
3	7690	1709.07	1820.93	1682.79
3.25	8251	1822.70	1942.00	1794.67
3.5	8769	1928.00	2054.19	1898.35
3.75	9252	2026.64	2159.28	1995.47
4	9704	2119.05	2257.74	2086.46
4.25	10128	2206.05	2350.44	2172.13
4.5	10529	2288.39	2438.17	2253.20
4.75	10907	2366.39	2521.28	2330.00
5	11266	2446.71	2606.85	2409.08
5.25	11608	2502.28	2666.06	2463.80
5.5	11614	2266.13	2414.45	2231.29
5.75	9045	1597.58	1702.14	1573.01
6	7044	1286.14	1370.32	1266.37
6.25	5486	997.15	1062.42	981.82
6.5	4273	776.99	827.85	765.04
6.75	3328	605.13	644.74	595.83
7	2592	471.24	502.09	464.00
7.25	2018	366.90	390.91	361.26
7.5	1572	285.85	304.56	281.46
7.75	1224	222.50	237.06	219.08
8	953	173.25	184.59	170.58
8.25	742	N/A	N/A	N/A
8.5	578	N/A	N/A	N/A
8.75	450	N/A	N/A	N/A
9	351	N/A	N/A	N/A

Table 4.3.4: C2P τ investigation input ($AgNO_3$)

Input	Value
V_D	0.00006033m^3
V_A	0.000116767m^3
λ	0.0281767s^{-1}
Y_D	0.6506
Q	0.0011772m^3/s
tau	Variable
Y_A	2.01518E-09
E	2.45 MeV

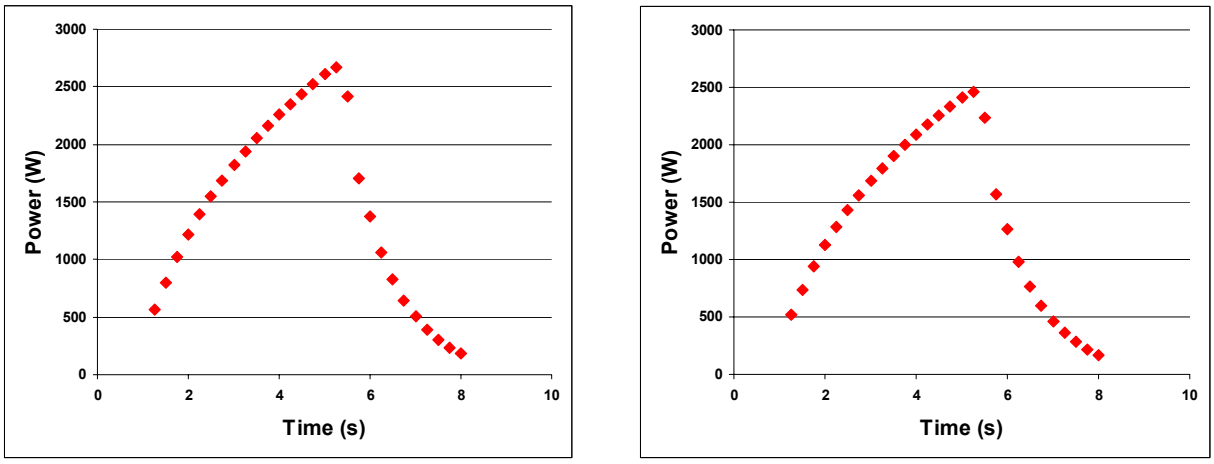

Increase Decrease

Figure 4.3.2: C2P τ investigation ($AgNO_3$)

Figure 4.3.2 reveals that changing the τ value does little to the power response. The maximum calculated power is scaled slightly, but has minimal effect.

It should be noted that the effect of both τ and Q is dependent upon the half-life of the activation substance, since a shorter half-life would imply that a lower τ and higher Q would be needed for equivalent results.

To complete the investigation into the behavioral dependence of the power response against certain variables, the effect of flow velocity should be investigated. This investigation is

important, because flow velocity is an easily adjustable value, depending mainly on the power setting of the pump, and flow velocity can always be adjusted. Flow velocity will alter both the Q and the τ, where the relationship is directly proportional for Q (i.e. $Q \propto v$) and inversely proportional for τ (i.e. $\tau \propto \frac{1}{v}$). The velocity was increased by a factor of three (36 m/s), then decreased by a factor of three (4 m/s). These results are shown in Table 4.3.5, and graphically in Figure 4.3.3, for input values as given in Table 4.3.6.

Table 4.3.5: C2P v investigation ($AgNO_3$)

	v (m/s)----------	12	36	4
	Q(m^3/s)----------	0.001177188	0.003531564	0.000392396
	tau (s)----------	0.75	0.25	2.25
Time (s)	**Count-rate (s^{-1})**	**Power (W)**		
0.25	2	N/A	N/A	N/A
0.5	1	N/A	N/A	N/A
0.75	3	N/A	N/A	N/A
1	25	N/A	N/A	N/A
1.25	1562	532.56	1175.44	331.70
1.5	2838	746.22	1924.95	347.69
1.75	3917	958.39	2582.03	418.72
2	4852	1141.72	3153.02	472.98
2.25	5677	1305.08	3658.38	522.64
2.5	6414	1452.12	4110.96	568.06
2.75	7081	1586.10	4521.46	610.02
3	7690	1709.07	4896.94	648.90
3.25	8251	1822.70	5243.18	685.02
3.5	8769	1928.00	5563.26	718.81
3.75	9252	2026.64	5862.17	750.71
4	9704	2119.05	6142.00	780.66
4.25	10128	2206.05	6404.82	809.09
4.5	10529	2288.39	6653.47	835.90
4.75	10907	2366.39	6888.03	862.25
5	11266	2446.71	7115.28	899.07
5.25	11608	2502.28	7325.03	868.16
5.5	11614	2266.13	7104.67	589.24
5.75	9045	1597.58	5354.19	328.79
6	7044	1286.14	4201.46	330.46
6.25	5486	997.15	3270.73	243.09
6.5	4273	776.99	2547.66	190.30
6.75	3328	605.13	1984.21	148.18
7	2592	471.24	1545.33	115.35

Table 4.3.5 (continued)

Time (s)	Count-rate (s^{-1})	Power (W)		
7.25	2018	366.90	1203.13	89.84
7.5	1572	285.85	937.27	70.01
7.75	1224	222.50	729.71	54.43
8	953	173.25	568.16	42.41
8.25	742	N/A	N/A	N/A
8.5	578	N/A	N/A	N/A
8.75	450	N/A	N/A	N/A
9	351	N/A	N/A	N/A

Table 4.3.6: C2P v investigation input ($AgNO_3$)

Input	Value
V_D	0.00006033m^3
V_A	0.000116767m^3
Λ	0.0281767s^{-1}
Y_D	0.6506
Q	Variable
Tau	Variable
Y_A	2.01518E-09
E	2.45 MeV

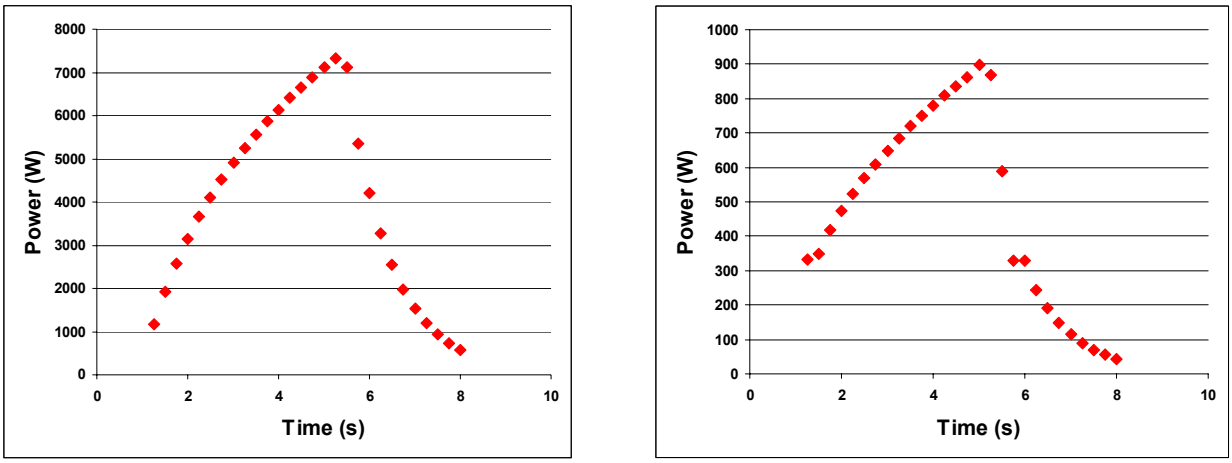

Increase Decrease

Figure 4.3.3: C2P v investigation ($AgNO_3$)

It can be seen from Figure 4.3.3 that altering the flow velocity results in a response curve that resembles only altering the volumetric flow-rate. This is especially visible when the flow

velocity is decreased, as in Figure 4.3.3 (Decrease). This result is expected, since the individual investigations of Q and τ revealed that the calculated power has a much higher dependence on Q.

4.4 C2P Behavioral Analysis – H_2O

The investigation presented in Section 4.3 was repeated for H_2O with the same count-rate sample. For the volumetric flow-rate investigation, the results are shown in Table 4.4.1, and graphically in Figure 4.4.1, with input values shown in Table 4.4.2.

Table 4.4.1: C2P Q Investigation (H_2O)

	Diameter (in)------	0.44	1	0.21
	v (m/s)----------	12	61.98	2.73
	Q (m^3/s)----------	0.0011772	0.0060805	0.00026815
Time (s)	**Count-rate (s^{-1})**	**Power (W)**		
0.25	2	N/A	N/A	N/A
0.5	1	N/A	N/A	N/A
0.75	3	N/A	N/A	N/A
1	25	N/A	N/A	N/A
1.25	1562	57.35	204.19	31.48
1.5	2838	80.45	348.31	28.92
1.75	3917	103.36	472.53	34.44
2	4852	123.16	580.40	38.01
2.25	5677	140.79	675.74	41.34
2.5	6414	156.67	761.03	44.43
2.75	7081	171.13	838.33	47.31
3	7690	184.41	908.97	49.99
3.25	8251	196.68	974.09	52.48
3.5	8769	208.05	1034.25	54.83
3.75	9252	218.69	1090.40	57.07
4	9704	228.67	1142.96	59.16
4.25	10128	238.06	1192.30	61.16
4.5	10529	246.95	1238.97	63.04
4.75	10907	255.37	1282.98	64.96
5	11266	264.03	1325.22	68.39
5.25	11608	270.05	1365.05	61.75
5.5	11614	244.72	1341.68	30.43
5.75	9045	172.62	1025.18	13.13
6	7044	138.93	801.61	20.08

Table 4.4.1 (continued)

Time (s)	Count-rate (s^{-1})	Power (W)		
6.25	5486	107.72	624.22	13.49
6.5	4273	83.94	486.21	10.65
6.75	3328	65.37	378.68	8.29
7	2592	50.91	294.93	6.45
7.25	2018	39.64	229.61	5.03
7.5	1572	30.88	178.87	3.92
7.75	1224	24.04	139.27	3.04
8	953	18.72	108.43	2.37
8.25	742	N/A	N/A	N/A
8.5	578	N/A	N/A	N/A
8.75	450	N/A	N/A	N/A
9	351	N/A	N/A	N/A

Table 4.4.2: C2P Q investigation input (H_2O)

Input	Value
V_D	0.00006033m^3
V_A	0.000116767m^3
Λ	0.0972156s^{-1}
Y_D	0.6983
Q	Variable
Tau	0.75 sec
Y_A	3.08772E-08
E	14.1MeV

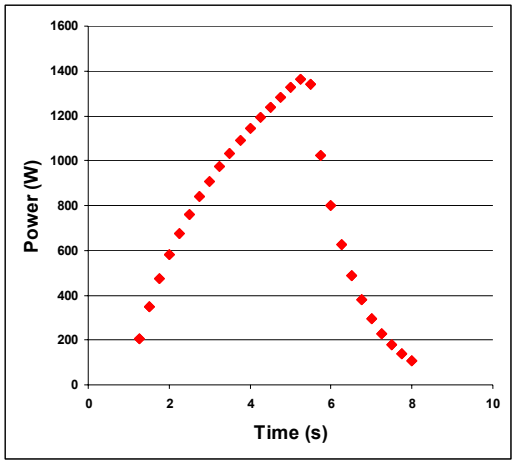

Increase

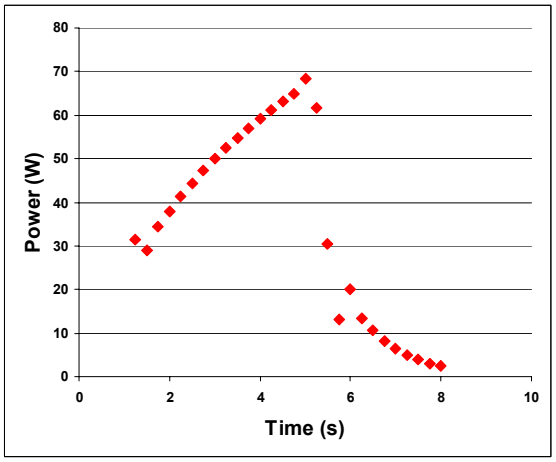

Decrease

Figure 4.4.1: C2P Q investigation (H_2O)

Behavior differences between the $AgNO_3$ volumetric flow-rate investigation and H_2O investigation are indistinguishable, with the exception of scaling. The calculated H_2O power is significantly smaller, resulting from the larger yield values. That is, assuming no change in flux, one would expect higher count-rate values when employing H_2O as the activation fluid.

The transport delay value, τ, was also investigated, and the results are shown in Table 4.4.3, graphically in Figure 4.4.2, where the input values are shown in Table 4.4.4.

Table 4.4.3: C2P τ investigation (H_2O)

	tau (s)----------	0.75	3	0.2
Time (s)	**Count-rate (s^{-1})**		**Power (W)**	
0.25	2	N/A	N/A	N/A
0.5	1	N/A	N/A	N/A
0.75	3	N/A	N/A	N/A
1	25	N/A	N/A	N/A
1.25	1562	57.35	71.38	54.37
1.5	2838	80.45	100.12	76.26
1.75	3917	103.36	128.63	97.98
2	4852	123.16	153.27	116.74
2.25	5677	140.79	175.22	133.46
2.5	6414	156.67	194.98	148.51
2.75	7081	171.13	212.98	162.22
3	7690	184.41	229.50	174.81
3.25	8251	196.68	244.77	186.44
3.5	8769	208.05	258.91	197.21
3.75	9252	218.69	272.16	207.31
4	9704	228.67	284.58	216.76
4.25	10128	238.06	296.27	225.67
4.5	10529	246.95	307.33	234.09
4.75	10907	255.37	317.81	242.07
5	11266	264.03	328.59	250.29
5.25	11608	270.05	336.08	255.99
5.5	11614	244.72	304.55	231.98
5.75	9045	172.62	214.83	163.63
6	7044	138.93	172.90	131.70
6.25	5486	107.72	134.06	102.11
6.5	4273	83.94	104.46	79.57
6.75	3328	65.37	81.35	61.97
7	2592	50.91	63.35	48.26
7.25	2018	39.64	49.33	37.57
7.5	1572	30.88	38.43	29.27
7.75	1224	24.04	29.91	22.79

Table 4.4.3 (continued)

8	953	18.72	23.29	17.74
8.25	742	N/A	N/A	N/A
8.5	578	N/A	N/A	N/A
8.75	450	N/A	N/A	N/A
9	351	N/A	N/A	N/A

Table 4.4.4: C2P τ investigation input (H_2O)

Input	Value
V_D	$0.00006033m^3$
V_A	$0.000116767m^3$
Λ	$0.0972156s^{-1}$
Y_D	0.6983
Q	$0.0011772m^3/s$
Tau	Variable
Y_A	3.08772E-08
E	14.1MeV

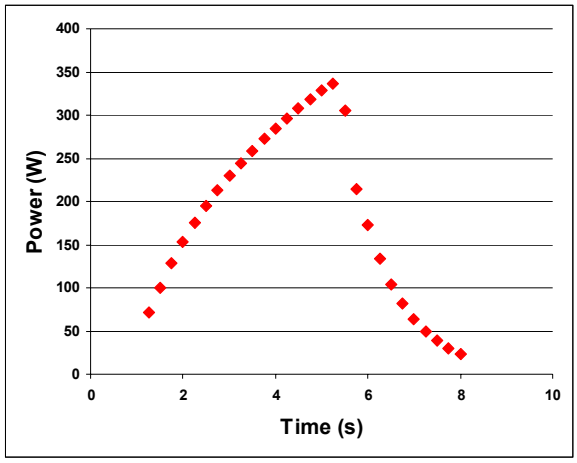

Increase

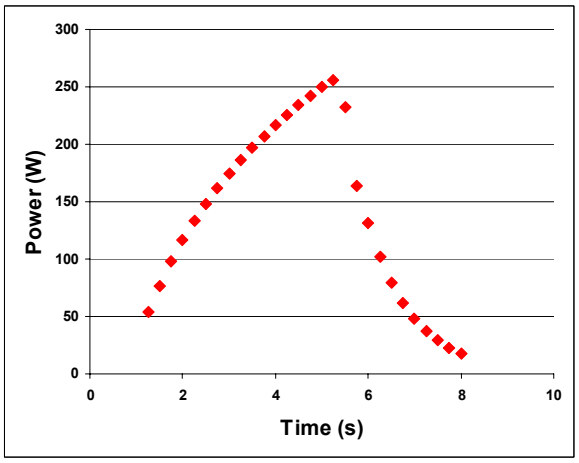

Decrease

Figure 4.4.2: C2P τ investigation (H_2O)

Once again, both H2O and AgNO3 investigations yielded very similar results, only noticeably differing in the scale.

Finally, the fluid velocity was investigated, and the results are shown in Table 4.4.5, graphically in Figure 4.4.3, where input values are shown in Table 4.4.6.

Table 4.4.5: C2P v investigation (H_2O)

	v (m/s)----------	12	36	4
	Q(m^3/s)----------	0.001177188	0.003531564	0.000392396
	tau (s)----------	0.75	0.25	2.25
Time (s)	**Count-rate (s^{-1})**	**Power (W)**		
0.25	2	N/A	N/A	N/A
0.5	1	N/A	N/A	N/A
0.75	3	N/A	N/A	N/A
1	25	N/A	N/A	N/A
1.25	1562	57.35	121.68	40.07
1.5	2838	80.45	199.30	42.23
1.75	3917	103.36	267.35	50.91
2	4852	123.16	326.48	57.56
2.25	5677	140.79	378.81	63.65
2.5	6414	156.67	425.67	69.22
2.75	7081	171.13	468.18	74.36
3	7690	184.41	507.07	79.12
3.25	8251	196.68	542.92	83.55
3.5	8769	208.05	576.07	87.68
3.75	9252	218.69	607.02	91.59
4	9704	228.67	636.00	95.25
4.25	10128	238.06	663.21	98.73
4.5	10529	246.95	688.96	102.02
4.75	10907	255.37	713.25	105.24
5	11266	264.03	736.78	109.70
5.25	11608	270.05	758.50	106.13
5.5	11614	244.72	735.73	72.71
5.75	9045	172.62	554.49	40.88
6	7044	138.93	435.11	40.70
6.25	5486	107.72	338.72	30.01
6.5	4273	83.94	263.84	23.49
6.75	3328	65.37	205.49	18.29
7	2592	50.91	160.04	14.24
7.25	2018	39.64	124.60	11.09
7.5	1572	30.88	97.06	8.64
7.75	1224	24.04	75.57	6.72
8	953	18.72	58.84	5.23
8.25	742	N/A	N/A	N/A
8.5	578	N/A	N/A	N/A
8.75	450	N/A	N/A	N/A
9	351	N/A	N/A	N/A

Table 4.4.6: C2P v investigation input (H_2O)

Input	Value
V_D	$0.00006033m^3$
V_A	$0.000116767m^3$
Λ	$0.0972156s^{-1}$
Y_D	0.6983
Q	Variable
Tau	Variable
Y_A	3.08772E-08
E	14.1MeV

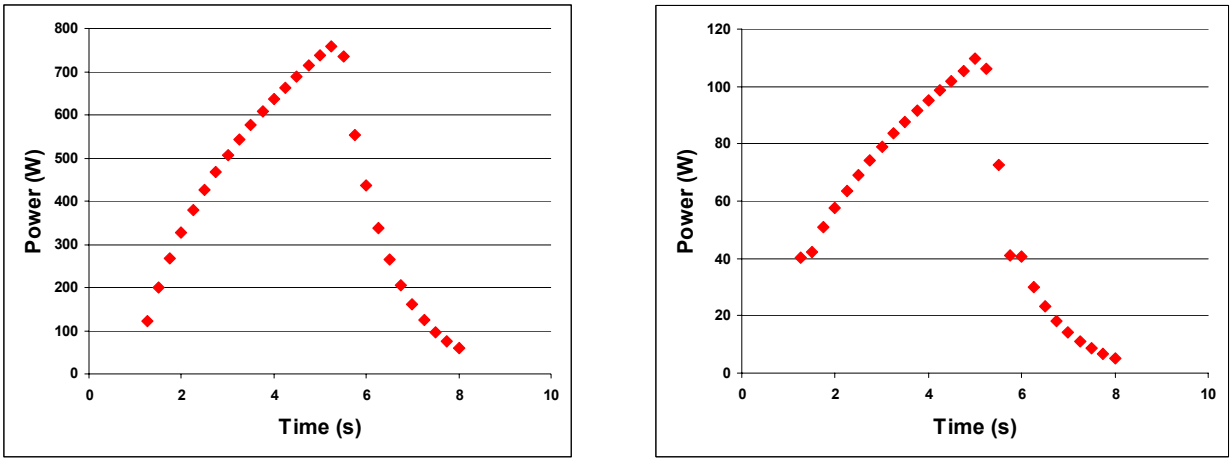

Increase Decrease

Figure 4.4.3: C2P v investigation (H_2O)

Once more, the behavioral analysis is indistinguishable between H_2O and $AgNO_3$, with an exception to scaling.

5 Conclusions and Suggestions for Future Work

This research has shown that a real-time fusion power monitor device based on the neutron activation of a circulating fluid is feasible for the DIII-D toroidal reactor, and hence it is feasible for similar future fusion reactors such as ITER. The components are quite simple and can be employed don the sampling modules, known as DiMES, residing on the bottom divertor of MCF reactors like DIII-D. The DiMES device is a very appealing location for fluid irradiation, with minimal modification needed to construct a functional fluid irradiation volume. Piping with diameter of around half an inch can be employed to circulate the fluid. It will be necessary to install a pump with enough power to ensure turbulent flow, since research performed by the Japanese "JAERI" group has shown turbulent flow to be optimal. For detecting the 14.1 MeV neutrons from D-T fusion reactions the activation fluid would be H_2O where irradiated oxygen produces the isotope of interest. For detecting the 2.45MeV neutrons from D-D fusion reactions it was shown that water diluted with silver nitrate is well suited, where the irradiation of silver is of interest. A delay tank is to be added to ensure sufficient radionuclide decay before the fluid is recirculated, however, it was shown that a cylindrical tank with inner dimensions of two feet in diameter and three feet in height will be sufficient. A well-design NaI scintillation detector was shown to be the optimal detector, producing detection yields of 65.06% for $AgNO_3$ fluid and 69.83% for H_2O fluid.

The Count-to-Power program, "C2P," was written for near real-time operation of the device, with small delays resulting from fluid transport and numerical techniques. The program should be stable for most all count-rate behaviors exhibited by the irradiation fluid, with the only weakness being relatively large disjoint behaviors in count-rate. Given a sample input, both H_2O and $AgNO_3$ activation fluids were shown to have very similar output power trends. A behavioral

analysis performed by changing first volumetric flow-rate, then transport delay, and finally fluid velocity showed that the device is quite sensitive to volumetric flow-rate, but not transport delay. Thus, regardless of which activation fluid is employed, when constructing this device, more attention is needed for such matters as pipe diameter and flow velocity than pipe length; unless if one is considering time resolution, which the JAERI team showed is minimized for shorter transport time.

A proposal for future work is to construct a neutron power measuring device based on the monitoring of a circulating activation fluid. The neutron source need not be a fusion reactor. This will provide data to benchmark the C2P program. The C2P program can be further modified by constructing a Visual Basic program to control its input and output. The physical model can be enhanced by studying the magnetic effect on circulated silver nitrate. This is especially interesting for fluid within the activation volume, where velocity profiles may indicate low velocity zones, thus low momentum zones to force the $AgNO_3$ to continue to circulate. Providing one's self with such assumptions as a power profile would also be an interesting course of study. It would allow for a forward calculation model, as well as error calculation. The DIII-D divertor is subjected to high heat fluxes; studying their effect would provide further insight. Of course, ultimately it would be interesting to construct this d1evice on the DIII-D and test its performance for verification and benchmarking.

References

[1] Lamarsh, John R. and Anthony J. Baratta. *Introduction to Nuclear Engineering.* 3rd Ed. Prentice Hall. 2001.

[2] Chen, Francis F. *Introduction to Plasma Physics and Controlled Fusion*. 2nd Ed. Springer. 2006.

[3] Fusion Technology Institute. 15 Mar 2007. <http://fti.neep.wisc.edu/neep602/LEC24/IMAGES/Fusion.GIF>.

[4] NASA. 15 Mar 2007. <http://imagine.gsfc.nasa.gov/Images/teachers/posters/elements/booklet/energy.jpg>.

[5] International Thermonuclear Experimental Reactor. 15 Mar 2007. <http://www.iter.org/>

[6] General Atomics. 5 Mar 2007. <http://fusion.gat.com/global/Visitor>.

[7] SolidWorks Express. 5 Mar 2007. <http://www.solidworks.com/swexpress/pages/mar05/PU_GeneralAtomics.html>.

[8] Bourham, Mohammed. General discussion. 5 Dec 2006.

[9] Combs, S. K., L. R. Baylor, C. R. Foust, T. C. Jernigan, P. M. Anderson, and J. I. Robinson. "New Pellet Injection Schemes on DIII-D." 5 Mar 2007. <http://www.ornl.gov/sci/fed/pellet/combs_sofe99.pdf>.

[10] Taylor, Peter. "RE:neutron spectrum in DiMES." Reply e-mail to Brandon Clark. 6 Dec 2006.

[11] Wong, C. P. C., R. J. Bastaz, D. G. Whyte, W. R. Wampler, and W. P. West. "Erosion Results From DiMES and Design Implications to ITER and Starlite." July 1996.

[12] Nahm, Meredith and Crystal Buchanan. "Design of Multi-Diagnostic Dimes." Senior design. Spring 1993.

[13] Kaneko, Junichi, Yoshitomo Uno, Takeo Nishitani, Fujio Maekawa, Teruya Tanaka, Yoshinari Shibata, Yujiro Ikeda, and Hiroshi Takeuchi. "Technical feasibility study on a fusion power monitor based on activation of water flow." Review of Scientific Instruments. 72.1 (January 2001).

[14] Walker, Christopher. "FW:ITER Question: water activation for power monitor." Reply e-mail to Brandon Clark. 21 Nov 2006.

[15] Rizk, R. A. M., K. Verghese, and R. P. Gardner. "A Model for Continuous On-stream Neutron Activation Analysis." Nuclear Geophysics. 4.3 (1990): 389-396.

[16] Taylor, Peter. "RE:DIII-D modeling." Reply e-mail to Brandon Clark. 8 Jan 2007.

[17] Gardner, Robin P. General discussion. 5 Feb 2007.

[18] T-2 Nuclear Information Service. LANL. 6 Dec 2006. <http://t2.lanl.gov/cgi-bin/endlnk?ag109h>.

[19] Ernest O. Lawrence Berkeley National Laboratory. 6 Dec 2006. <http://ie.lbl.gov/education/isotopes.htm>.

[20] Salt Lake Metals. 6 Dec 2006. <http://www.saltlakemetals.com/Solubility_Of_Silver_Nitrate.htm>

[21] Knoll, Glenn F. Radiation Detection and Measurement. 3rd Ed. John Wiley & Sons, Inc., 2000.

[22] Saint-Gobain. "Monoline Scintillation Detectors with Integrally Mounted PMT." 2002.

[23] Burden, Richard L. and J. Douglas Faires. Numerical Analysis. 7th Ed. Brooks/Cole, 2001.

[24] Griffiths, D.V. and I.M. Smith. Numerical Methods for Engineers. 2nd Ed. Chapman & Hall/CRC, 2006.

Appendices

Appendix I

Count-to-Power Program

```
program c2p

!!!!!!!!!!!!!!!!!!!!!!!!!!!!!!!!!!!!!!!!!!!!!!!!!!!!!!!!!!!!!!!!!!!!!!!!!!!!
!  Programmer:  Brandon Clark
!
!  Purpose:
!    To calculate the power from a radiation source assuming counts come from a detector
!    monitoring an activated fluid flow with delay tank.
!
!  Files:
!    c.txt             -  [time, detector count-rate]
!    constants.txt     -  constants:
!                           1.) state
!                           2.) VD
!                           3.) VA
!                           4.) lambda
!                           5.) YD
!                           7.) Q
!                           8.) tau
!                           9.) YA
!                           10.) E
!    results.txt       -  program results (output)
!
!  Arrays
!    C           -  [time, detector count-rate]
!    ND          -  [time, radionuclide density in detection volume]
!    NA          -  [time-tau, radionuclide density in activation volume]
!    R           -  [time-tau, production rate of radionuclide]
!    A           -  [time-tau, source activity]
!    P           -  [time-tau,
!    NDprime     -  [time, numerical derivative of radionuclide density in detection volume]
!    NAprime     -  [time-tau, numerical derivative of radionuclide density in activation volume]
!    prime       -  [time, derivative of given array]
!
!  Variables:
!    VD          -  detection volume {m^3}
!    VA          -  activation volume {m^3}
!    lambda      -  decay constant {s^-1}
!    YD          -  detection volume yield, equal to the multiplication of detector yield and decay
!                   occurrence rate of particle/ray
!    Q           -  volumetric flow rate {m^3/s}
```

```
!     tau            -  elapsed time of fluid flow from activation volume to detection volume {s}
!     YA             -  activation volume yield, equal to the multiplication of source yield,
!                       macroscopic absorption cross-section, and activation volume divided by
!                       activation volume surface area
!     E              -  energy released per decay {MeV}
!     state          -  "1" = non-steady-state
!                       "2" = steady-state
!!!!!!!!!!!!!!!!!!!!!!!!!!!!!!!!!!!!!!!!!!!!!!!!!!!!!!!!!!!!!!!!!!!!!!!!!!!!!!

Implicit Double Precision (a-z)

REAL, DIMENSION(10000,2) :: C,ND,NA,R,A,P,NDprime,NAprime,prime
REAL, DIMENSION (20) :: arb

real :: VD,VA,lambda,YD,Q,tau,YA,E,state
integer :: i=0,nvals,status

OPEN (unit=1,file='c.txt',status='old',action='read', &
                          IOSTAT=status)
OPEN (unit=2,file='constants.txt',status='old',action='read', &
                          IOSTAT=status)
OPEN (unit=3,file='results.txt',status='replace')

100 FORMAT (F10.3,1X,F12.3,1X,F30.5,1X,F10.4,1X,F30.5,1X,F20.4,1X,E20.10,1X,&
                              E20.10)
200 FORMAT (3X,A5,11X,A1,21X,A10,9X,A9,17X,A10,14X,A8,10X,A8,14X,A8)

Do
  i=i+1
  READ (2,*,IOSTAT=status) arb(i) !arbitrary array
  If (status /= 0) Exit
End Do

state=arb(1)        !dimensionless
VD=arb(2)           !m^3
VA=arb(3)           !m^3
lambda=arb(4)       !s^-1
YD=arb(5)           !dimensionless
Q=arb(6)            !m^3/s
tau=arb(7)          !s
YA=arb(8)           !dimensionless
E=arb(9)            !MeV

i=0
Do
  i=i+1
```

```
  READ (1,*,IOSTAT=status) C(i,1), C(i,2) !time,counts
  If (status /= 0) Exit
End Do

nvals=i-1

!~~~~~~~~~~~ Equation 1 ~~~~~~~~~~~~~~~

Do i=1,nvals
  ND(i,1)=C(i,1)
  ND(i,2)=C(i,2)/(VD*lambda*YD)
End Do

!~~~~~~ Take Derivative of ND ~~~~~~~~

If (state == 1) Then
  CALL fivepoint (ND,nvals,prime)

  Do i=1,nvals
    NDprime(i,1)=prime(i,1)
    NDprime(i,2)=prime(i,2)
  End Do
End If

!~~~~~~~~~~~ Equation 2 ~~~~~~~~~~~~~~~

If (state == 1) Then
  NA(1,1)=C(1,1)-tau
  NA(1,2)=0
  NA(2,1)=C(2,1)-tau
  NA(2,2)=0
  NA(nvals-1,1)=C(nvals-1,1)-tau
  NA(nvals-1,2)=0
  NA(nvals,1)=C(nvals,1)-tau
  NA(nvals,2)=0

  Do i=3,nvals-2
    NA(i,1)=C(i,1)-tau
    NA(i,2)=(VD*NDprime(i,2)+lambda*VD*ND(i,2)+Q*ND(i,2))/(Q*exp(-lambda*tau))
  End Do
Else
  Do i=1,nvals
    NA(i,1)=C(i,1)-tau
    NA(i,2)=(lambda*VD*ND(i,2)+Q*ND(i,2))/(Q*exp(-lambda*tau))
  End Do
End If
```

```
!~~~~~~ Take Derivative of NA ~~~~~~~~

If (state == 1) Then
  CALL fivepoint (NA,nvals,prime)

  Do i=1,nvals
    NAprime(i,1)=prime(i,1)
    NAprime(i,2)=prime(i,2)
  End Do
End If

!~~~~~~ Equation 3 ~~~~~~~~

If (state == 1) Then
  R(1,1)=NA(1,1)
  R(1,2)=0
  R(2,1)=NA(2,1)
  R(2,2)=0
  R(3,1)=NA(3,1)
  R(3,2)=0
  R(4,1)=NA(4,1)
  R(4,2)=0
  R(nvals-3,1)=NA(nvals-3,1)
  R(nvals-3,2)=0
  R(nvals-2,1)=NA(nvals-2,1)
  R(nvals-2,2)=0
  R(nvals-1,1)=NA(nvals-1,1)
  R(nvals-1,2)=0
  R(nvals,1)=NA(nvals,1)
  R(nvals,2)=0

  Do i=5,nvals-4
    R(i,1)=NA(i,1)
    R(i,2)=VA*NAprime(i,2)+lambda*VA*NA(i,2)+Q*NA(i,2)
  End Do
Else
  Do i=1,nvals
    R(i,1)=NA(i,1)
    R(i,2)=lambda*VA*NA(i,2)+Q*NA(i,2)
  End Do
End If

!~~~~~~ Equation 4 ~~~~~~~~

Do i=1,nvals
```

```
   A(i,1)=NA(i,1)
   A(i,2)=R(i,2)/YA
End Do

!~~~~~~ Equation 5 ~~~~~~~~

Do i=1,nvals
   P(i,1)=NA(i,1)
   P(i,2)=A(i,2)*E*1.60217646E-13   !Watts
End Do

!~~~~~~ Write Results ~~~~~~~~

write (3,200) 't (s)','C','ND (#/m^3)','t-tau (s)','NA (#/m^3)',&
            'R (s^-1)','A (s^-1)','P (Watt)'

Do i=1,nvals
   write(3,100) C(i,1),C(i,2),ND(i,2),NA(i,1),NA(i,2),R(i,2),A(i,2),P(i,2)
End Do

Close (Unit=1)
Close (Unit=2)
Close (Unit=3)

write (*,*) 'Count-to-Power Complete'
write (*,*) 'Reminder: Values of 0 are invalid'

End Program

!~~~~~~ Five-Point Numerical Differentiation ~~~~~~~~

subroutine fivepoint (data,nvals,prime)
Implicit Double Precision (a-z)

INTEGER, INTENT(IN) :: nvals
REAL, DIMENSION(10000,2), INTENT(IN) :: data
REAL, DIMENSION(10000,2), INTENT(INOUT) :: prime
REAL :: h
INTEGER :: i

Do i=1,nvals
   prime(i,1)=data(i,1)
End Do

h=data(2,1)-data(1,1)
```

```
prime(1,2)=0
prime(2,2)=0
prime(nvals-1,2)=0
prime(nvals,2)=0

Do i=3,nvals-2
  prime(i,2)=(1/(12*h))*(-25*data(i-2,2)-8*data(i-1,2)+8*data(i+1,2)-data(i+2,2))
End Do

End Subroutine
```

Appendix II

Five-point Formula Derivation

Consider the data to have uniform spacing, h, so the formula will take the form,

$$f'(x_o) \approx g[h, f(x_o - 2h), f(x_o - h), f(x_o), f(x_o + h), f(x_o + 2h)] \qquad \text{(Eq. A.2.1)}$$

Taking the Taylor series expansion about $f(x_o)$ yields

$$f(x_o - 2h) = f(x_o) - 2hf'(x_o) + \frac{4h^2}{2!} f''(x_o) - \frac{8h^3}{3!} f'''(x_o) + \frac{16h^4}{4!} f^{iv}(x_o) - \frac{32h^5}{5!} f^{v}(x_o)... \qquad \text{(Eq. A.2.2)}$$

$$f(x_o - h) = f(x_o) - hf'(x_o) + \frac{h^2}{2!} f''(x_o) - \frac{h^3}{3!} f'''(x_o) + \frac{h^4}{4!} f^{iv}(x_o) - \frac{h^5}{5!} f^{v}(x_o)... \qquad \text{(Eq. A.2.3)}$$

$$f(x_o + h) = f(x_o) + hf'(x_o) + \frac{h^2}{2!} f''(x_o) + \frac{h^3}{3!} f'''(x_o) + \frac{h^4}{4!} f^{iv}(x_o) + \frac{h^5}{5!} f^{v}(x_o)... \qquad \text{(Eq. A.2.4)}$$

$$f(x_o + 2h) = f(x_o) + 2hf'(x_o) + \frac{4h^2}{2!} f''(x_o) + \frac{8h^3}{3!} f'''(x_o) + \frac{16h^4}{4!} f^{iv}(x_o) + \frac{32h^5}{5!} f^{v}(x_o)... \qquad \text{(Eq. A.2.5)}$$

which can be treated as a system of equations

$$\begin{bmatrix} 1 & 0 & 0 & 0 \\ 0 & 1 & 0 & 0 \\ 0 & 0 & 1 & 0 \\ 0 & 0 & 0 & 1 \end{bmatrix} \begin{bmatrix} f(x_o - 2h) \\ f(x_o - h) \\ f(x_o + h) \\ f(x_o + 2h) \end{bmatrix} = \begin{bmatrix} 1 & -2 & 1 & -4/3 & 2/3 & -4/15 \\ 1 & -1 & 1/4 & -1/6 & 1/24 & -1/120 \\ 1 & 1 & 1/4 & 1/6 & 1/24 & 1/120 \\ 1 & 2 & 1 & 4/3 & 2/3 & 4/15 \end{bmatrix} \begin{bmatrix} f(x_o) \\ hf'(x_o) \\ h^2 f''(x_o) \\ h^3 f'''(x_o) \\ h^4 f^{iv}(x_o) \\ h^5 f^{v}(x_o) \end{bmatrix}$$

The system is solved algebraically to eliminate $f''(x_o)$, $f'''(x_o)$, and $f^{iv}(x_o)$, then is solved for $f'(x_o)$, yielding the five-point formula

$$f'(x_o) = \frac{1}{12h}[f(x_o - 2h) - 8f(x_o - 1) + 8f(x_o + 1) - f(x_o + 2h) + \frac{1}{30}h^4 f^{v}(\xi)]$$

Where for the design x=t and $h = \Delta t$ [24].

Appendix III

MCNP Input – Activation

```
c     Created on: Wednesday, January 10, 2007 at 11:38
    1     0         -4 -6 7  $DiMES fluid region
    2     0         (6 -3 -4 7 ):(-3 -7 5 ) $DiMES ambient region
    3     0         -1 2 4 8  $DIII-D vessel chamber region
    4     0         -8  $Source region
    5     0         -2 :-5 :(-4 3 ):(1 4 ) $leftover

c    D-shape chamber is not possible, creating pseudo with torus and cylinder.
c    Vertical minor radius of torus has been enlongated so the bottom is more
c    realistic.  Plane is used to create bottom of D-shape
    1        tz 0 0 0 140.2842 145 $Elliptical Torus for pseudo D-shape cha
                 102.9208
    2       c/z 0 0 95.885  $Cylinder for pseudo D-shape chamber
    3       c/z 148 0 4.08  $DiMES outer cylinder
    4        pz -142.3162  $Top of DiMES (outer and activation), bottom of torus
    5        pz -157.5562  $Bottom of outer DiMES cylinder
    6       c/z 148 0 2.2876  $DiMES activation cylinder
    7        pz -149.4187  $Bottom of DiMES activation cylinder
    8        tz 0 0 0 170 1 1  $Source torus

imp:n             1 3r                      0  $ 1, 5
sdef    ERG=2.45 POS=0 0 0 CEL=4 RAD=D1 EXT=D2 AXS=0 0 1
si1     169.9 170.1
si2     0.1
f1:n    4
fs1     -6
c1      0 1
nps     100000000
```

MCNP Input – Detection Geometry 1

Note that there exist separate input files for each detection scheme (i.e. detecting one beta, two, or gamma). However, the alteration between input files is elementary, thus only one input is shown for each detection geometry.

```
c     Created on: Friday, January 12, 2007 at 13:23
    1     2   -3.67 -3 5 -6  $Detector region
    2     0         (-2 8 -9 10 ):(-2 -10 4 ):(-2 9 -7 ) $Detector ambient
    3     1 -2.05512 11 -1 -7 4  $Detection tank region
    4     0         1 :7 :-4  $Leftover
    5     4    -2.7 (10 -5 -8 ):(5 -6 -8 3 ):(6 -9 -8 ) $Detector wall (1/16")
    6     3   -8.03 -11 2 -7 4  $Detection tank wall (1/8")

    1       c/z 0 0 3.71968  $Detection tank (outer)
    2       c/z 0 0 2.7178  $Detection tank (inner)
    3       c/z 0 0 2.54  $Detector (note: 2" X 2")
    4        pz 0  $Detection tank (bottom)
    5        pz 0.1778  $Detector (bottom)
    6        pz 5.2578  $Detector (top)
    7        pz 5.4356  $Detection tank (top)
    8       c/z 0 0 2.6162  $Detector wall (cyclinder)
    9        pz 5.334  $Detector wall (top)
```

```
   10        pz 0.1016  $Detector wall (bottom)
   11       c/z 0 0 2.794  $Detection tank wall

mode  p
m1    47000.04p      -0.42359  $fluid
      7000.04p         -0.055 8000.04p       -0.48416 1000.04p       -0.03725
m2    11000.04p     -0.153373  $detector
      53000.04p     -0.846627
m3    26000.04p      -0.70995  $SS304
      24000.04p         -0.18 28000.04p         -0.08 25000.04p         -0.02
      7000.04p         -0.001 16000.04p       -0.0003 6000.04p        -0.0008
      14000.04p       -0.0075 15000.04p      -0.00045
m4    13000.04p             1  $Al
imp:p             1 2r                        0            1 1r            $ 1, 6
sdef    ERG=0.6577622 POS=0 0 2.7178 CEL=3 RAD=D1 EXT=D2 AXS=0 0 1
si1     2.795 3.71967
si2     2.7177
f8:p    1
nps     1000000
```

MCNP Input – Detection Geometry 2

```
c     Created on: Friday, January 12, 2007 at 13:23
    1     2   -3.67 -3 5 -6  $Detector region
    2     0         (8 -12 -2 ):(12 -7 -2 11 ) $Detector ambient
    3     1 -2.05512 (4 -8 -1 ):(8 -7 -1 2 ) $Detection tank region
    4     0         (1 -7 ):(7 11 -6 ):6 :-4  $Leftover
    5     4    -2.7 (-6 5 3 -9 ):(-5 10 -9 ) $Detector wall (1/16")
    6     3   -8.03 (12 -10 -11 ):(10 -6 -11 9 ) $Protective layer

    1       c/z 0 0 2.8551505  $Detection tank (outer)
    2       c/z 0 0 2.6924254  $Detection tank (inner)
    3       c/z 0 0 2.54  $Detector (note: 2" X 2")
    4        pz 0  $Detection tank (bottom)
    5        pz 3.9624254  $Detector (bottom)
    6        pz 9.0424254  $Detector (top)
    7        pz 5.710301  $Detection tank (top)
    8        pz 3.81  $Top of fluid, below detector
    9       c/z 0 0 2.6162  $Detector wall (cyclinder)
   10        pz 3.8862254  $Detector wall (bottom)
   11       c/z 0 0 2.6924  $Protective layer
   12        pz 3.8100254  $Protective layer (bottom)

mode  p
m1    47000.04p      -0.42359  $fluid
      7000.04p         -0.055 8000.04p       -0.48416 1000.04p       -0.03725
m2    11000.04p     -0.153373  $detector
      53000.04p     -0.846627
m3    26000.04p      -0.70995  $SS304
      24000.04p         -0.18 28000.04p         -0.08 25000.04p         -0.02
      7000.04p         -0.001 16000.04p       -0.0003 6000.04p        -0.0008
      14000.04p       -0.0075 15000.04p      -0.00045
m4    13000.04p             1  $Al
imp:p             1 2r                        0            1 1r            $ 1, 6
sdef    ERG=0.6577622 POS=0 0 2.8551505 CEL=3 RAD=2.854 EXT=D1 AXS=0 0 1
si1     2.854
f8:p    1
nps     1000000
```

MCNP Input – Detection Geometry 3

```
c     Created on: Tuesday, February 06, 2007 at 16:26
    1     1 -2.05512 1 -2 -5  $fluid region
    2     3    -2.7 (1 -2 5 -6 ):(2 -3 -6 ) $lining (0.01in)
    3     2   -3.67 (1 -3 6 -7 ):(3 -4 -7 ) $crystal
    4     0         -1 :4 :7  $ambient

    1        pz 0  $bottom
    2        pz 7.62  $top of fluid region
    3        pz 7.6454  $top of lining
    4        pz 10.16  $top of crystal
    5       c/z 0 0 1.5875  $side of fluid region
    6       c/z 0 0 1.6129  $side of lining
    7       c/z 0 0 3.81  $side of crystal

mode  p
m1    47000.04p      -0.42358  $fluid
      7000.04p         -0.055 8000.04p       -0.48416 1000.04p       -0.03725
m2    11000.04p    -0.1533733  $detector
      53000.04p     -0.846627
m3    13000.04p             1  $lining
imp:p            1 2r                      0  $ 1, 4
sdef    ERG=0.6577622 POS=0 0 3.81 CEL=1 RAD=1.587 EXT=D1 AXS=0 0 1
si1     3.8
f8:p    3
nps     1000000
```